MEASUREMENT OF THE COMPLEX DYNAMIC RIGIDITY OF RECENT MARINE SEDIMENTS

Gregory Allen Engel

NAVAL POSTGRADUATE SCHOOL
Monterey, California

THESIS

MEASUREMENT OF THE COMPLEX DYNAMIC RIGIDITY OF RECENT MARINE SEDIMENTS

by

Gregory Allen Engel

Thesis Co-Advisors:
O. B. Wilson
R. S. Andrews

December 1972

Measurement of the Complex Dynamic Rigidity of Recent Marine Sediments

by

Gregory Allen Engel
Lieutenant Junior Grade, United States Navy
B.S., United States Naval Academy, 1971

Submitted in partial fulfillment of the
requirements for the degree of

MASTER OF SCIENCE IN OCEANOGRAPHY

from the

NAVAL POSTGRADUATE SCHOOL
December 1972

ABSTRACT

The dynamic rigidity of 17 samples of continental terrace clayey-silt sediments has been measured in the laboratory using a viscoelastometer in the frequency range of 7 to 60 kHz. The method involves the propagation of torsional waves on a rod and measuring the effects of shear loading imparted to the rod when imbedded in a sediment. Values of the real component of rigidity range from 1.6 X 10^6 dynes/cm^2 to 2.1 X 10^7 dynes/cm^2. Values of the imaginary component of rigidity range from 2.0 X 10^5 dynes/cm^2 to 4.1 X 10^7 dynes/cm^2. No clear-cut dependence of rigidity upon frequency is observed. Both real and imaginary components of rigidity are analyzed by plotting the data as a function of various other mass-physical properties, including: density, porosity, compressional wave speed, sand-silt-clay percentages, vane shear strength, and the product of density and sound speed squared. These analyses substantiate research done by other workers indicating that both real and imaginary components of rigidity exhibit trends with some of the mass-physical properties.

TABLE OF CONTENTS

I. INTRODUCTION---------- 8

II. THEORY AND METHOD OF MEASUREMENT---------- 10

A. GENERAL---------- 10

B. RESONANCE METHOD---------- 12

III. EQUIPMENT AND PROCEDURES---------- 14

A. EQUIPMENT---------- 14

B. PROCEDURES---------- 16

C. SEDIMENT PREPARATION---------- 16

IV. LIMITATIONS ON RESULTS---------- 20

V. RESULTS AND DISCUSSION---------- 24

VI. CONCLUSIONS AND RECOMMENDATIONS---------- 30

COMPUTER PROGRAMS---------- 73

BIBLIOGRAPHY---------- 77

INITIAL DISTRIBUTION LIST---------- 79

FORM DD 1473---------- 81

LIST OF TABLES

I. Station Location, Water Depth, and Bottom Water Temperature---------- 31

II. Textural Analysis of 6-inch Core Sections---------- 32

III. Textural Analysis of 14-inch Core Sections (Interpolated)---------- 33

IV. Mass-Physical Properties of 6-inch Core Sections---------- 34

V. Mass-Physical Properties of 14-inch Core Sections (Interpolated)---------- 35

VI. Mass-Physical Properties of 14-inch Core Sections---------- 36

VII. Acoustic Properties---------- 37

VIII. Values of Viscoelastic Calibration Coefficients K_1 and K_2---------- 38

IX. Standard Deviation and Variation of Dynamic Rigidity Parameters---------- 39

LIST OF FIGURES

1. Coordinates for Shear Wave Propagation, Equivalent Electrical Circuit of Rod-Transducer System------------------ 41

2. Cut-Away View of Viscoelastometer and Shear Transducer Polarities--- 42

3. Block Diagram of Equipment for Resonant Method-------------- 43

4. Coring Station Locations------------------------------------ 44

5. Sectioning of Cores--- 45

6. Plot of Sand/Silt/Clay Ratios for Each Core Section Analyzed--- 46

7. Resonant Frequency as a Function of Temperature Probe 1, Mode 1--- 47

8. Resonant Frequency as a Function of Temperature Probe 1, Mode 2--- 48

9. Resonant Frequency as a Function of Temperature Probe 1, Mode 3--- 49

10. Resonant Frequency as a Function of Temperature Probe 1, Mode 4--- 50

11. Resonant Frequency as a Function of Temperature Probe 2, Mode 1--- 51

12. Resonant Frequency as a Function of Temperature Probe 2, Mode 2--- 52

13. Resonant Frequency as a Function of Temperature Probe 2, Mode 3--- 53

14. Resonant Frequency as a Function of Temperature Probe 4, Mode 1--- 54

15. Resonant Frequency as a Function of Temperature Probe 4, Mode 2--- 55

16. Resonant Frequency as a Function of Temperature Probe 4, Mode 3--- 56

17. G_1 as a Function of Density--------------------------------- 57

18. G_1 as a Function of Porosity-------------------------------- 58

19. G_1 as a Function of Sound Speed---------------------------- 59

20. G_1 as a Function of Percent Sand--------------------------- 60

21. G_1 as a Function of Percent Silt--------------------------- 61

22. G_1 as a Function of Percent Clay--------------------------- 62

23. G_1 as a Function of Vane Shear Strength-------------------- 63

24. G_1 as a Function of Density and Sound Speed Squared-------- 64

25. G_2 as a Function of Density-------------------------------- 65

26. G_2 as a Function of Porosity------------------------------- 66

27. G_2 as a Function of Sound Speed---------------------------- 67

28. G_2 as a Function of Percent Sand--------------------------- 68

29. G_2 as a Function of Percent Silt--------------------------- 69

30. G_2 as a Function of Percent Clay--------------------------- 70

31. G_2 as a Function of Vane Shear Strength-------------------- 71

32. G_2 as a Function of the Product of Density and Sound Speed Squared-- 72

Acknowledgements

The author wishes to express his gratitude to Professor O. B. Wilson and Professor R. S. Andrews of the Naval Postgraduate School for their guidance and aid in the research described in this report. The author also wishes to thank Lieutenant Commander Robert J. Cepek, USN, and Mr. Ken Smith for their support and the associated research of this report. Additionally, the author gratefully acknowledges the assistance of Mr. Larry Leopold of San Jose State College and his students in coring operations at sea.

Use of the USNS BARTLETT (T-AGOR-13) was essential in obtaining core samples for research. The project received support through contract with the Office of Naval Research, Ocean Science and Technology Division.

I. INTRODUCTION

Because of the growing importance of sound reflections from the ocean floor during recent years, an increasing amount of study has been directed toward marine sediments with the goal of improving the accuracy of predicting the acoustic reflection characteristics of the ocean floor, taking into account variations in sediment constituency and mass-physical properties.

Various acoustic models of the ocean floor have been used in these efforts. Most assume a multilayered liquid model, the simplest of which is the two-fluid model where the sediment is considered to be a layer of fluid with a density and sound speed different from that of the overlying sea water. Such models are often successful because of low rigidities and shear-wave velocities in surficial sediments [8]. Somewhat more sophisticated models include the effects of inhomogeneities in the bottom materials and the effects of a bottom which has a shear elasticity. A still more realistic model for sediments is that of a viscoelastic solid. Several studies have shown that although elastic model equations adequately define the velocities of compressional and shear waves, they do not, of course, account for absorption, which is also important [9]. For this reason a viscoelastic model involving complex Lamé constants and including the generation of shear waves upon reflection and absorption of the waves is favored [9]. An additional problem is the difficulty of evaluating the Lamé constants for various oceanic areas and soft sediment types. Evaluation of the constants is known by only three direct methods: (1) the Stonely wave technique [10], which is limited to low frequencies; (2) use of torsional wave vibration [7]; or (3) a torsional wave viscoelastometer [11, 5, 2].

Research conducted by Hutchins [11] at the Naval Postgraduate School demonstrated the feasibility of measuring the complex shear modulus or dynamic rigidity of simulated ocean sediments. The method involves measuring the effects of shear waves generated in the sediment due to the propagation of torsional waves along the length of a cylindrical rod immersed in the sediment. Hutchins worked with kaolinite-water mixtures in the narrow frequency range of 38.3 to 38.9 KHz. Cohen [5] used an improved model viscoelastometer and extended the frequency range to 5.8 to 38 KHz. Using saturated samples of kaolinite and bentonite clays, Cohen demonstrated that these soft, undispersed, simulated sediments do have measurable shear moduli which are independent of frequency. Bieda [2] developed a totally immersible viscoelastometer and used it to determine the complex rigidity of actual ocean sediments obtained from the continental terrace. Bieda analyzed the sediments for mass-physical properties and demonstrated that both real and imaginary components of rigidity exhibit trends with some of those properties.

The purpose of the research here reported was to test and develop a newer model viscoelastometer, possibly suitable for in situ measurement, and to apply it to the measurement of dynamic rigidity of real ocean sediments. The following sections describe the theory of measurement, the equipment and procedures, sample collection and preparation, the limitations of the method, and results of the various rigidity determinations. A discussion of results and recommendations for future research are then presented.

II. THEORY AND METHOD OF MEASUREMENT

A. GENERAL

The determination of the sediment's shear modulus and viscosity is made from measurements of the reaction to shear waves which radiate into the sediment from the surface of a cylindrical metal rod which is oscillating in torsion. This torsional motion, generated by a piezoelectric crystal transducer mounted within the metal rod, is at a frequency for resonance of the waves propagating in the rod. Although the shear waves in the sediment are usually too highly attenuated to allow investigation of their propagation, the reaction to this radiation is detected by electrical measurements on the piezoelectric crystal.

The geometry of the torsional oscillation and the resulting shear waves is indicated by the sketch in Figure 1. The rod axis about which simple harmonic torsional oscillations take place is parallel to the y-direction. At the circumference of the rod, displacements are along the circumference, the x-direction. Shear waves in the surrounding medium, generated by this motion, propagate radially outward, along the z-direction.

Following Mason's development [13] and McSkimin's hypothesis [15], if it can be assumed that shear waves propagating radially outward into a fluid in contact with the rod have a wave-length which is very small compared to the radius of curvature of the rod, and that the amplitude of these waves is rapidly attenuated, then the waves can be treated essentially as plane waves propagating in a fluid having a shear viscosity coefficient, η. Plane shear waves of the form

$$U_x = U_o e^{-\alpha z} e^{i(\omega t - kz)} \qquad (1)$$

propagating into an infinite medium are assumed. For a Newtonian fluid,

$$\alpha = k = \sqrt{\frac{\pi f \rho}{\eta}} \tag{1A}$$

where f = frequency, ρ = density and η = shear viscosity coefficient. U_o is the initial amplitude.

If the sediment were solid, its shear modulus would be given by:

$$G = \tau/S \tag{2}$$

where τ is shear stress, and S is shear strain. In a liquid sediment the shear viscosity coefficient would be $\eta = \tau/\dot{S}$, where $\dot{S} = \partial S/\partial t$, and is thus the shear velocity.

Assuming a viscoelastic sediment, both G and η are complex [14].

$$G_c = G_1 + iG_2 \tag{3}$$

$$\eta_c = \eta_1 - i\eta_2 \tag{4}$$

$G_2 = 0$ in a perfectly elastic solid; $\eta_2 = 0$ in a Newtonian fluid. For plane, simple, harmonic waves of angular frequency ω,

$$\eta_c = \tau/i\omega S = -iG_c/\omega \tag{5}$$

Hence, $G_1 = \omega\eta_2$, and $G_2 = \omega\eta_1$, where ω is the angular frequency.

The specific acoustic load impedance of the sediment on the rod, Z, is given by

$$Z = \eta_c U_x$$

and for plane shear waves is given by

$$Z' = \sqrt{\pi f \rho_{sed} \eta_c}(1 + i) = R + iX \tag{6}$$

where

R = specific acoustic resistance of the sediment

X = specific acoustic reactance of the sediment

ρ_{sed} = density of the sediment

Substituting η_c in its complex form and separating real and imaginary parts yields

$$\eta_1 = 2RX/\omega\rho_{sed}, \quad \eta_2 = (R^2 - X^2)/\omega\rho_{sed}; \tag{7}$$

$$G_1 = (R^2 - X^2)/\rho_{sed}, \quad G_2 = 2RX/\rho_{sed}. \tag{8}$$

Determination of shear moduli and viscosities then reduces to measuring R and X.

B. RESONANCE METHOD

In this method, based on work by Mason [13], the torsional transducer-rod combination is driven in a continuous wave mode, exciting standing waves on the probe. The rod-transducer system is represented approximately by an equivalent electrical circuit consisting of the capacitance, C, in parallel with a series RLC circuit which arises from the motions of the system. When excited at the frequency of mechanical resonance the electrical conductance, G_E, is a maximum. At each resonance mode the input electrical conductance is measured first with the probe suspended in a vacuum, then with the probe imbedded in the medium under study. This allows calculation of the change in equivalent parallel electrical resistance at resonance, ΔR_E. The change in the resonance frequency for each mode, Δf, is also recorded. Mason has shown that [13]:

$$\Delta R_E = K_1 R_T \quad \text{and} \quad \Delta f = K_2 X_T$$

where K_1 and K_2 are constants which are a function of fixed physical parameters. These constants are determined by making measurements with

the probe suspended in Newtonian fluids of known viscosity. In a Newtonian fluid, $\eta_2 = 0$; therefore $R_T = X_T$. R_T and X_T are the components of the total impedance presented to the rod by the sediment. After substitution, K_1 and K_2 reduce to

$$K_1 = \frac{\dfrac{1}{G_{F\ell}} - \dfrac{1}{G_{vac}}}{l\sqrt{\rho_{F\ell}\ \pi\ f_{F\ell}\ \eta_1}} \tag{9}$$

$$K_2 = \frac{f_{vac} - f_{F\ell}}{l\sqrt{\rho_{F\ell}\ \pi\ f_{F\ell}\ \eta_1}} \tag{10}$$

where

G = electrical conductance

l = length of viscoelastometer submerged

ρ = density

f = frequency

η_1 = viscosity in poise

III. EQUIPMENT AND PROCEDURES

A. EQUIPMENT

The driving transducer is a hollow barium titanate ceramic cylinder 0.5 inches in diameter and 1.5 inches in length. It is constructed from an axially-polarized cylinder which is cut into two parts along the longitudinal axis and rejoined following inversion of one half-section and insertion of two electrode grids (Figure 2). This produces a shear-type oscillation in the ceramic when electrically excited. A description of this method can be found in Mason [14].

Of the three laboratory viscoelastometers utilized, two were stainless steel and one was constructed of a constant modulus alloy, NI-Span-C. As in earlier probes used by Bieda the transducer is located at the center giving a maximum point of stress for all resonant modes. In contrast to Bieda's probes, however, the newer model viscoelastometers have the transducers completely within the viscoelastometer body (Figure 2).

Stainless steel was used because it does not corrode when immersed in sediment for long periods. NI-Span-C was being tested for its more stable characteristics. Each rod is 20.32 cm long, 1.78 cm in diameter, and cut at mid-section to allow insertion of the ceramic oscillator. Both sections of the rod are polished. The NI-Span-C rods were heat-treated to achieve constant modulus before assembly. The transducer is glued to each half of the viscoelastometer to join the rod. Small holes drilled in the internal perimeter of the rod allow the glue to penetrate and help to ensure proper bonding. A 5-mil thick nylon mesh gasket was used in the glue joint to control glue joint thickness. The electrical leads to the transducer are carried out through small holes at the joint

between the two halves of the metal rod. After the bonding glue had cured, the joining seam and the electrical connections were given a thin coat of epoxy to prevent leakage to the interior of the probe and to provide electrical insulation. At the top of the viscoelastometer a small hole was drilled. A few strands of stainless steel thread were then inserted, being held in place with low temperature solder. To the other end of the thread a small pinch clip was soldered for support purposes.

On the exterior of each a probe near the seam a small coating of varnish was applied and a number scribed on each viscoelastometer. Probe 1 and Probe 2 are stainless steel. Probe 4 is the NI-Span-C alloy.

The vacuum calibrating was done within copper canisters with an inside diameter of 6.3 cm. "O" rings prevented leakage at the metal to metal junctions of the canister. The vacuum canister containing the probe was then placed in a thermally controlled water bath at 20.0°C. Water temperature was monitored with a digital thermometer. To determine the temperature dependence of the resonant frequencies of the probes in vacuum the water bath temperature was raised to 25°C. A sufficient period was allowed for the equipment to stabilize and the resonant frequencies of each mode were recorded. A similar process was again followed for 20°C, 15°C, 10°C and 5°C. The results of these studies are shown in Figures 7-16.

The resonance method equipment configuration is shown in Figure 3. The sinusoidal signal generated by the oscillator is connected to the counter and the admittance meter in parallel. The five-decade counter was set for either a 10-sec or 1-sec gate in order to provide a precision in the determination of the resonant frequency consistent with that with which the settings could be made.

Compressional wave speed in the sediment cores was measured with a sediment velocimeter obtained from the Pacific Support Group of the Naval Oceanographic Office. The velocimeter uses a two transducer method to measure the time delay for sound transmission through the diameter of the core samples. Computation of the velocity in the sediment is accomplished by comparing the time delay through the sediment filled core liner to the time delay in an identical core filled with distilled water at the same temperature. The equation is:

$$C_{sed} = C_w \left(\frac{1}{1 - \frac{C_w \Delta t}{d}} \right)$$

where C_{sed} is the sediment compressional wave speed, C_w is the sound speed in distilled water, Δt is the comparable time delay, and d is the inside core diameter.

B. PROCEDURES

At resonance the viscoelastometer is driven in a standing mode and resonance frequencies as well as input electrical conductances at resonance are recorded. Measurements made in a vacuum, and later in Newtonian fluids, permit calculation of K_1 and K_2 of the probes (Program KCALC). A Brookfield Viscometer is utilized to obtain values of the shear viscosity coefficient for the calibrating fluid. The K values are obtained for each mode of vibration for each probe in the various calibrating fluids. The K values from the various calibrating fluids for each mode are then averaged for each probe. The final averaged values of K are listed in Table VIII.

C. SEDIMENT PREPARATION

The supply of sediment cores were obtained from operations conducted aboard USNS BARTLETT (T-AGOR-13) on 11-13 May 1972 in the area illustrated

in Figure 4. The area was chosen so as to insure that samples would contain minimal amounts of sand-sized particles. The area is on the Monterey Submarine Fan where previous coring and dredging has yielded samples of a low sand content [17]. Minimization of sand content is necessary as particles in this size range are comparable to the wavelength of the shear waves at the frequencies produced by the viscoelastometer. This invalidates the assumption of homogeneity.

The samples retrieved were gravity cores. Upon being brought aboard the cores were cut into alternate 6-inch and 14-inch sections using the heated element method. This technique utilizes a soldering gun with a modified tip and positioning rings to cut the core liner only. A thin wire was passed through the sediment to separate the sections. As soon as possible the 6-inch sections were subjected to vane shear strength measurements in the ship's dry lab using a Wykeham-Farrance Vane Shear Machine with modifications. Output graphs of the torque vs. rotation at sediment failure were recorded. These vane shear strengths were then correlated with the values of dynamic rigidity obtained from viscoelastic measurements. A more detailed description of cutting, coring and vane shear procedures is given by Cepek [4].

The 14-inch core sections were capped and stored upright in the ship's wet lab refrigerator until they could be transferred to the Sea Floor Acoustics Laboratory at the Naval Postgraduate School. Once transferred they were placed in a salt water bath under refrigeration at 5°C until at such time they could be used for the viscoelastic study. A salt water bath was chosen to prevent dessication of the sediment through the core liner.

The 6-inch cores were tested for determination of porosity. Porosity is the percentage of voids per unit volume. Porosity of the 6-inch cores was calculated by Cepek [4] and the porosity of the 14-inch sections was determined from interpolation (Table V).

Laboratory measurements of wet density and water content were conducted simultaneously using prescribed procedures [12] and calculated by Cepek. Again the values of the wet density and water content of the 14-inch core sections were obtained from interpolation of the 6-inch core section values (Table V).

All sediment samples from the BARTLETT cruise were subjected to grain size analysis. The sieve analysis method was performed on the coarse fraction of each sample ($<4\phi$), and the pipette method was used for each sample after the coarse fraction had been removed. Again, results and description of the analysis are given by Cepek. For the 14-inch core sections each sediment sample was inspected upon probe removal. Coarse particles were never found in the vicinity of viscoelastic penetration.

To prepare the 14-inch core sections for insertion of the viscoelastic probe, the sediment samples were removed from their 5°C salt water bath and immersed in a 20°C bath. After temperature stabilization was attained compressional wave speed measurements were made. The sediment core was then uncapped and a hollow coring tube of 1.75 cm diameter was slowly pushed vertically through the center of the sediment core. This provided a bore hole of a slightly smaller diameter than the viscoelastometer into which the viscoelastometer could be pressed with a minimum of sediment disturbance. No support for the probe was required as the sediment was sufficiently strong to maintain the viscoelastometer in position. With the electrical leads in position the core was then

recapped and taped to prevent moisture loss. The electrical conductivity of the sediment was sufficient to provide an electrical ground connection for the probe.

The recapped core section was then placed in a thermally controlled container and electrical connections were made. Between eight and ten hours were required before stable and consistent measurements could be taken.

To extract the probe from the sediment a cork plunger was utilized. The probe and sediment were then removed and the sediment inspected for sand content in the vicinity of the probe.

IV. LIMITATIONS ON RESULTS

One goal of the development of this viscoelastometer in these studies was to achieve values for K_1 and K_2 which were frequency independent. Complete independence was not accomplished; however, the stability was much greater than in previous studies with earlier model viscoelastometers. Various viscosity oils, ranging from 10 to 300 poise, were used with the higher viscosities giving better results. It was found that the viscoelastometers were unable to distinguish the lighter viscosity fluids from non-loaded conditions accurately and these results were neglected. A narrow range of higher viscosity fluids will give much better results for consistent values of K_1 and K_2. Average values of the constants were used to compute dynamic rigidities (Table V).

Two critical assumptions of theory development are that the wavelength of the shear wave in the medium is much smaller than the radius of curvature of the probe and that the amplitude decays to a small value in an insignificant distance compared to the radius of the rod. The shear wave speed, C_s, is calculated using the formula:

$$C_s = \sqrt{G/\rho}$$

where G is the absolute value of the complex rigidity and ρ is the sediment density. The wavelength of the shear wave is then:

$$\lambda = C_s/f$$

where f is the frequency. The wavelength in the stiffer sediments at the lowest mode is about .15 cm while the radius of curvature of the rod is about 0.9 cm. This assumption is therefore assumed valid at all frequencies of interest.

The absorption coefficient, α (Equations 1 and 1A), for a typical case is about 15 cm^{-1}. This implies that the shear wave amplitude is reduced to 1/e of its initial value in about 0.07 cm, again, significantly smaller than the radius of the rod.

Another important assumption for linearizing the wave equation is that the amplitudes of motion are essentially infinitesimal. To determine the validity of this assumption, the displacement of the viscoelastometer was optically measured at resonance through a high-powered microscope. In an unloaded state (air) and driven at 50 volts, the maximum observed peak to peak displacement amplitude was about one micron at the lowest mode. Imbedded in sediment while resonating under normal conditions (driven at 3 volts) the amplitude will be considerably less than 0.06 microns. Thus the assumption of a small amplitude holds true.

Since no sand-sized particles were found in the vicinity of the viscoelastometers during sediment analysis, no anomalous behavior is expected for this reason.

There were other problems which affected the accuracy of the results. One was the mechanical degradation of the viscoelastometers in service. The following case is one example. Early in the test program, after completing a sequence of measurements in a number of cores, viscoelastometer No. 1 was rechecked in the vacuum chamber. Corrosion of the support hook had required that this be replaced, which involved heating one end of the rod to the temperature for melting soft solder. It was observed that the resonance frequencies had shifted significantly, as much as 95 Hz for one mode, since the first calibration tests. Although the heating process was done carefully, this may have changed the elastic properties of the rod or have disturbed the glue joints. In any case, this casts some uncertainties on the results gained with this probe.

Another problem involved leakage of water into the transducer compartment of the torsional probes. This appeared to be due to repeated immersions and washings which degraded the epoxy-resin seal at the press fit joint between the two halves and at the electrical lead-in wires. The disturbance to the measurements caused by the resulting electrical leakage was usually severe enough that this trouble was detected almost immediately. In most cases, the trouble was corrected by scraping away the epoxy-resin seal, drying by pumping in a vacuum and resealing.

Additional reasons for uncertainties in the obtained results are the structural damage caused by the core collection method and by possible core dessication during storage. The cores were gravity cores and a considerable amount of sediment disturbance is assumed. Analysis utilizing Probe 1 was commenced shortly after the cores were retrieved. Analysis utilizing Probe 2, however was not carried out for another five months. Even though the cores were kept in a 5°C salt water bath, various amounts of dessication and compaction were noted to have occurred. Through qualitative handling the sediments in this second group were found to be firmer, which one would expect to be associated with increased values of rigidity. This also implies that the textural sediment analysis which was undertaken when the cores were fresh will not strictly apply to the measurements from Probe 2.

To determine errors due to uncertainties in the measurements, the standard deviation of each input parameter was determined (Table IX). These standard deviations were then used to recalculate the values of dynamic rigidity from which the percentage variation could be computed. This resulted in a maximum possible relative error of about 50% in G_1, and about 72% in G_2. Such a large error is attributable mainly to a

sensitivity to values of the resonant frequency and conductance. An uncertainty of 0.67 Hz in the probe's resonant frequency in a sediment results in a 37% uncertainty in G_1. A deviation of this amount can be caused by temperature, variation, instrument error, measurement error or a combination of them.

V. RESULTS AND DISCUSSION

The original intent of the current viscoelastometer production was to develop an in situ probe. Temperature dependence, fragile physical composition, and variability of calibration constants indicate this model to be improperly suited for in situ measurements however. The dependence of the resonant frequency upon temperature is shown in Figures 7-16. The variability is not constant among the resonant frequency modes as indicated by the values of K_1 and K_2 (Table VIII). However, the NI-Span-C alloy rod appears to be the least variable and may be suited for in situ research if a proper set of temperature correction tables is developed.

Due to problems described previously in Section IV, the results are divided into two groups. Group 1 contains the measurements made with Probe 1 on fresh sediment cores but limited by the problems encountered in probe degradation. Group 2 contains measurements made with Probe 2 in which the cores were noted for dessication and compaction while the measuring viscoelastometer remained in good working condition.

The results of the experimental measurements and analyses are presented in Table VI. The magnitude of the real component of rigidity observed in these surficial continental terrace clayey-silt sediments range from 1.6×10^6 to 2.1×10^7 dynes/cm^2. Values of the imaginary components of rigidity range between 2.0×10^5 to 4.1×10^7 dynes/cm^2. Corresponding shear wave speeds calculated are between 12 and 57 m/sec. Bieda [2], who obtained cores from the same continental terrace area as those analyzed in this study, computed real components of rigidity from 6.5×10^5 to 2.6×10^7 dynes/cm^2. Observed imaginary components of rigidity ranged from 2.9×10^5 to 8.2×10^6 dynes/cm^2. Corresponding shear wave speeds

are from 7 to 40 m/sec giving good correlation to sediments from a similar area utilizing similar viscoelastometer techniques. The magnitudes of the rigidity are less than those reported by Hamilton et al [10], who derived a value of 1.6 X 10^8 dynes/cm^2 for sediments off San Diego utilizing Stoneley wave techniques. This difference in magnitude could be related to three factors [2]: (a) Monterey Bay sediments have been recently laid down at high deposition rates, allowing little time for cementation and/or compaction; (b) the rigidity could have been reduced due to sampling techniques; (c) the Stoneley wave technique may be affected by at least the first meter of sediment, yielding an averaging of the results in the upper meter of depth. Other researchers, however, have also obtained similar results confirming the existence of low rigidities. Anderson and Latham [1], in studying the dispersion of Rayleigh waves due to oceanic seismic activity, had to assume an extremely low sediment shear velocity range of 30 to 120 m/sec for a sediment layer 150 meters thick in order to obtain good correlation between theoretical models and experimental data. Davies [6], studying the dispersion of waves from explosions, obtained shear wave velocities from 50 to 190 m/sec for the upper 16 meters of sediment in the Indian Ocean. Gallagher and Nacci [7], using a torsional wave vibration method obtained values of 2.3 X 10^7 dynes/cm^2, results which are similar to those obtained in this report. Shear velocities and the concomitant rigidities cited by other researchers are considerably higher than those discussed here [9]. The probable reason for this involves sediments of firmer structure with stronger interparticle bonds.

In addition to rigidity, compressional sound speed, shear wave speed, ratio of sound speed in sediment to that in sea water at 20°C, and the

product of density and sound speed squared, ρc^2, were calculated (Tables VI and VII). The values of density, water content, vane shear strength, porosity, mean grain size, and the sand-silt-clay ratios were interpolated from the values obtained by Cepek [4] (Tables III and V).

Because of the physical breakdown of Probe 1, no certainty in the values of G_1 and G_2 is known, and the values are only relative when considered against each other. Comparisons of the values of G_1 and G_2 obtained from Probe 2 are also restricted because of the limited number of samples. Although these values are considered to be more reliable because no physical problems were encountered with Probe 2, G_1 and G_2 are presumed unrepresentative of the cores because of the sediment dessication and compaction noted earlier. When comparing the vane shear strengths obtained from core 6A by Cepek [4] to the values of the shear modulus obtained from Probe 1, however, the trends are in keeping with each other. It is suspected, therefore, that while the values of G_1 and G_2 are not representative of the fresh cores, the trends do depict the relative nature of the shear moduli of the sediments.

When comparing the real component of rigidity, G_1, to density (Figure 17), both Group 1 and 2 indicate an increase of G_1 with increasing density. There is no definite indication of G_1 of Group 1 with porosity (Figure 18) but there is a slight increase of G_1 of Group 1 with decreasing porosity. The same trends were noted by Bieda [2] in similar sediments and has also been observed by Hamilton [9]. Higher porosities lead to lower densities and lower dynamic rigidities due to fewer interparticle contacts in sands and clayey silts. An increase of rigidity with increasing density may also be caused by an increase in pressure and compaction which increase both properties. When comparing G_1 to sound speed (Figure

19) no determination of trends is attempted because of the small range of variability of the sound speed among the different core sections.

As was also noted by Bieda [2] there is no apparent relationship between G_1 of either probe and the percentages of sand (Figure 20) and silt (Figure 21). There is an observable increase in G_1 of Group 1 with an increasing percentage of clay (Figure 22). This is in contrast to the trends noted by Bieda [2] in similar sediments and Hamilton [9] in abyssal plain and hill sediments. Rigidity in fine-grained clayey sediments is dependent upon the cohesive interparticle contacts and bonds. Sediment analysis of Bieda's cores showed a high percentage of silt and a medium to low percentage of clay, the opposite of the analysis of the cores studied in this report (Table III). This is one possible reason for the reverse in observed trends.

As noted previously, vane shear tests (Figure 23) correlate agreeably with rigidity, with G_1 of Group 2 showing much stronger trends than G_1 of Group 1. In cores such as 6A where the alternate 14-inch sections were analyzed exclusively with Group 1, similar relationships between vane shear and G_1 are evident. Many workers in the field of soil mechanics still question the value of vane shear strength measurements but the observed trends of this report add support that there may be more factors common to rigidity and vane shear strength than sediment structure.

Comparison between G_1 and ρc^2 shows an increase with G_1 of Group 2 with increasing ρc^2. No attempt is made to compare G_1 of Group 1 with ρc^2. This trend is in agreement with Hamilton [9] who considers ρc^2 the best empirical index to rigidity in continental terrace and abyssal plain environments.

When comparing the trends observed by Bieda [2] and those of this report for similar continental terrace sediments, it appears that like

relationships are found except in the case of clay percentage. The trends observed for rigidity, density, porosity, and ρc^2 lend support to Bieda's assumption that these properties are interrelated and affect the rigidity collectively. The increased clay content of the samples studied is assumed to be a factor in the contrast of observed trends although the influences of cementation and the rate of deposition remain unstudied. The physical degeneration of Probe 1 is also assumed to affect the absolute values of G_1.

The imaginary component of rigidity, G_2, representative of the damping of wave energy, exhibits few visible trends when plotted against the various mass-physical properties. G_2 of Group 1 and Group 2 shows no general relationships with density (Figure 25), porosity (Figure 26), sound speed (Figure 27), percent clay (Figure 30), vane shear strength (Figure 31), or ρc^2 (Figure 32). Since these properties represented traits of elastic response this is expected. This same relationship was observed by Bieda [2].

Graphical plots of the values of G_2 as a function of percentage sand (Figure 28) show an increase of G_2 with increasing percent sand. One possible reason is that the size of the sand particles may correspond to the wavelength of the shear wave and some dispersion may have occurred. Another possibility is that in order for sand particiles to cause an increase in the rigidity they must be in close contact. In the case of low sand percentages and high porosities, as is indicated in this report, there is probably little particle to particle contact as the particles are surrounded by the viscoelastic clay, thus increasing the damping of the wave energy [9]. In comparing G_2 to percent silt (Figure 29) a similar increase of G_2 with increased silt percentages is observed, a trend

also noted by Bieda [2]. Looking specifically at G_2 of Group 1 as a function of clay content (Figure 30) a reversed trend of G_2 as compared to G_1 is observed. Thus, as the elastic rigidity increased with increasing silt there is an observable increase in G_2 with decreasing percentage silt.

If the G_2 data are compared with vane shear strength data, the values of G_2 gathered with both Group 1 and Group 2 increase varyingly with increasing shear strength. Since cohesion is the resistance to shear stresses and is considered to be an inherent property of fine-grained, clayey sediments [9], this reinforces the indication noted by Bieda that the imaginary component of rigidity is determined by properties related to cohesion and structure.

When G_2 is graphed against ρc^2 no trend is noted for G_2 of Group 2. A general increase of G_2 of Group 1 with an increase of ρc^2 is observed.

In a majority of core sections the imaginary component of rigidity is greater than the real component of rigidity. The deviation of the parameters used in computing G_2 was considerably larger than those involved with G_1 causing larger variations in the values of G_2 (Table IX). However, the larger G_2 values are believed to be caused by the sand and silt concentrations. Those core sections with a large G_2 were generally the same sections with an increased sand or silt content. This reinforces the indication that sand and silt directly influence the damping of the wave energy.

VI. CONCLUSIONS AND RECOMMENDATIONS

Although there is some doubt to the accuracy of the absolute values of the dynamic rigidity, it is concluded that the torsional wave viscoelastometer is probably giving valid results for the rigidities obtained. The assumptions inherent in the analysis of the data collected using this viscoelastometer also seem to be valid. Results correlate well with work done by previous researchers at the Naval Postgraduate School and with magnitudes reported for similar types of sediments by workers at other institutions using other measuring methods. The relationships between the rigidity and other sediment properties appear to be consistent with those reported by other workers.

Because this method also yields a value of the imaginary component of rigidity, which is related to the sound absorption process, this method should be developed further for use in sediment analysis. The current model viscoelastometer is unsuitable for in situ work because of the stable laboratory conditions required for sediment analysis. It is recommended that further research be done to correct the physical deficiencies which lead to probe failure. After final development of an in situ model, the present probe should be utilized for laboratory correlation analysis of cores brought back from the in situ sample area.

Comparison of values of dynamics shear modulus determined by various methods are needed for validation of the viscoelastometer technique. The relationships between rigidity and the other mass-physical properties, particularly sediment components, need further investigation.

Coring Station	Latitude N	Longitude W	Water Depth fm(m)	Bottom Water Temperature, °C
1B	36-45	123-16	1830(3347)	1.592
2	36-48	123-06	1745(3191)	1.803
3	36-48.5	123-20	1802(3295)	1.552
4	36-48	123-25	1900(3475)	1.548
5	36-44	123-28	1955(3575)	-
6A	36-40.5	123-17	1883(3444)	1.610
7	36-43.5	123-10	1917(3505)	1.630
8	36-44	123-01	1690(3091)	1.559

Table I. Station Location, Water Depth, and Bottom Water Temperature.

Core	Section	Depth in the Core inches	Mean Grain Size Ø	Sand %	Silt %	Clay %
1B	2	14	9.71	1.35	19.64	79.01
	4	34	9.66	1.09	20.92	77.99
	6	54	7.71	18.38	34.92	46.70
2	2	16	7.91	17.91	28.64	53.45
	4	36	9.72	.78	21.51	77.71
	6	53	9.71	.40	20.19	79.41
3	1	3	9.11	8.51	22.03	69.82
	3	24	7.73	31.40	19.36	49.24
	5	44	9.06	3.73	27.79	68.48
4	1	3	9.75	1.01	19.43	79.56
	3	23	9.78	.43	19.50	80.07
	5	44	9.12	6.22	24.97	68.81
5	1	3	9.53	1.35	22.79	75.86
	3	23	9.86	.48	17.19	82.33
	6	57	8.99	2.19	31.85	65.96
6A	1	3	9.73			
	2	8	9.80	.39	18.92	80.69
	4	28	9.46	.47	24.86	74.67
	6	48	8.64	3.25	37.76	58.99
	8	69	8.52	3.25	43.33	53.42
8	1	3	9.70	1.14	18.75	80.11
	3	23	9.59	.53	21.11	78.36
	5	43	9.48	.50	24.11	75.39

Table II. Textural Analysis of 6-inch Core Sections.

Core	Section	Depth in the core inches	Mean Grain Size Ø	Sand %	Silt %	Clay %
1B	2	7	NA	NA	NA	NA
	3	20	9.68	1.22	20.28	78.50
	5	40	8.68	9.73	27.92	62.35
2	1	8	NA	NA	NA	NA
	3	20	8.81	9.34	25.07	65.59
	5	40	9.71	.59	20.85	78.56
3	2	6	8.42	19.95	20.69	59.36
	4	26	8.39	17.56	22.57	59.87
4	2	6	9.76	.71	19.46	79.83
	4	26	9.45	3.32	22.23	74.45
5	2	6	9.79	.91	19.99	79.10
	4	26	9.57	1.05	22.08	76.87
	5	40	9.28	1.62	26.96	71.42
	7	60	NA	NA	NA	NA
6A	3	12	9.63	.43	21.79	77.78
	5	32	9.05	1.86	31.31	66.83
	7	52	8.58	3.25	40.54	56.31
7	2	6	9.67	.64	21.78	77.58
	4	26	9.35	1.53	23.16	75.31
	6	46	8.86	2.15	31.80	66.05
8	2	6	9.64	.83	19.93	70.24
	4	26	9.53	.51	22.61	76.88
	6	46	NA	NA	NA	NA

Table III. Textural Analysis of 14-inch Core Sections (Interpolated).

Core	Section	Wet Density g/cm^3	Water Content %	Shear Strength psi	Porosity %
1B	2	1.29	141	0.659	76.8
	4	1.34	126	0.839	75.1
	6	1.46	83	0.792	66.6
2	2	1.27	169	0.198	80.9
	4	1.26	168	0.676	78.6
	6	1.31	149	0.481	80.0
3	1	1.32	137	0.396	77.3
	3	1.33	128	1.024	75.2
	5	1.37	116	0.566	74.3
4	1	1.21	210	0.532	83.3
	3	1.31	141	0.668	77.6
	5	1.39	103	0.501	71.3
5	1	1.21	207	0.260	82.5
	3	1.31	142	0.591	77.7
	6	1.38	121	0.467	76.3
6A	1	1.21	207	0.504	82.7
	2	1.23	163	0.683	77.0
	4	1.34	125	0.611	75.3
	6	1.37	114	0.450	74.0
	8	1.38	101	0.417	70.3
8	1	1.33	211	0.127	84.6
	3	1.28	167	0.495	80.8
	5	1.30	141	0.586	76.9

Table IV. Mass-Physical Properties of 6-inch Core Sections.

Core	Section	Wet Density g/cm^3	Water Content %	Shear Strength psi	Porosity %
1B	1	1.27	NA	NA	NA
	3	1.31	133	0.749	75.9
	5	1.40	104	0.830	70.8
2	1	1.27	NA	NA	NA
	3	1.27	168	0.437	79.7
	5	1.29	158	0.578	79.3
3	2	1.32	132	0.710	76.2
	4	1.35	122	0.795	74.8
4	2	1.26	175	0.595	80.4
	4	1.35	122	0.584	74.5
5	2	1.26	174	0.425	80.1
	4	1.33	135	0.550	77.2
	5	1.35	128	0.508	76.7
	7	1.38	117	0.430	76.1
6A	3	1.28	149	0.647	76.2
	5	1.35	119	0.530	74.7
	7	1.38	108	0.434	72.1
8	2	1.31	189	0.311	82.7
	4	1.29	154	0.540	78.9
	6	1.31	134	NA	75.1

Table V. Mass-Physical Properties of 14-inch Core Sections (Interpolated).

Core	Section	Shear Wave Speed	ρc^2	G_1	G_2
		m/sec	(10^6 g-m^2/cm^2-sec^2)	(10^6 dynes/cm^2)	
1B	1	46.8	2.75	11.0	25.5
	3	21.1	2.71	5.8	.41
	5	51.0	3.02	21.1	29.7
2	1	12.1	2.81	7.7	16.9
	3				
	5		2.81		
3	2	18.1	2.95	2.3	3.9
	4	33.7	2.94	2.5	15.1
4	2	15.0	2.73	1.8	2.2
	4	18.1	2.92	4.4	.45
5	2	49.9	2.72	14.8	27.6
	4				
	5	15.6	2.93	3.3	.28
	7	20.0		4.5	3.4
6A	3	12.2	2.78	2.2	8.3
	5	21.5	2.93	4.1	4.7
	7	35.3	3.01	1.6	16.8
8	2	41.3	2.83	4.0	21.9
	4	20.2	2.79	5.1	.20
	6	57.2	2.83	11.3	41.3

Table VI. Mass-Physical Properties of 14-inch Core Sections.

Core	Section	Compressional Wave Speed m/sec	*C_{sed}/ C_{water} m/sec	Probable Fractional Error in C_{sed}
1B	1	1471.2	0.968	0.00099
	3	1471.1	0.968	
	5	1471.9	0.968	
2	1	1487.3	0.979	
	3	-	-	
	5	1471.1	0.968	
3	2	1490.8	0.981	
	4	1483.8	0.976	
4	2	1471.1	0.968	
	4	1471.2	0.968	
5	2	1471.5	0.968	
	4	-	-	
	5	1471.1	0.968	
	7	-	-	
6A	3	1471.2	0.968	
	5	1471.2	0.968	
	7	1478.9	0.973	
8	2	1472.2	0.969	
	4	1471.3	0.968	
	6	1471.7	0.968	

*Computed water speed is 1519.8 at 20°C and 35^{o}/oo.

Table VII. Acoustic Properties.

Frequency in kHz	K_1 (X 10^{-6})	K_2 (X 10^{-4})
PROBE 1		
7.94	22.1	9.6
24.18	2.9	4.8
41.01	1.4	4.8
57.98	.9	2.7
PROBE 2		
7.68	2.1	4.2
24.02	.2	3.7
59.70	.5	3.2
PROBE 4		
7.10	2.3	3.8
22.22	.3	2.6
55.18	.6	3.0

Table VIII. A Values of Viscoelastic Calibration Coefficients K_1 and K_2.

Parameter	Standard Deviation σ	Percent Variation in K_1	Percent Variation in K_2
PROBE 1			
Fvac	0.06 Hz	none	0.62
Foil	1.1 Hz	0.01	12.0
Goil	0.05 μ mhos	2.0	none
Fsed	4.7 Hz		
Gsed	0.01 μ mhos		
K_1	0.42 $(X10^{-6})$		
K_2	68.0 $(X10^{-6})$		
PROBE 2			
Fvac	0.20 Hz	none	1.0
Gvac	0.37 μ mhos	0.07	none
Foil	0.81 Hz	0.00	4.2
Goil	0.05 μ mhos	0.59	none
Fsed	0.67 Hz		
Gsed	0.06 μ mhos		
K_1	0.44 $(X10^{-6})$		
K_2	130.0 $(X10^{-6})$		
PROBE 3			
Fvac	0.14 Hz	none	0.96
Gvac	0.35 μ mhos	0.04	none
Foil	1.2 Hz	0.01	8.1
Goil	0.04 μ mhos	0.48	none

Table IX. Standard Deviation and Variation of Dynamic Rigidity Parameters.

Parameters	% η_1	% η_2	% G_1	% G_2
PROBE 1				
Fvac	0.78	0.12	0.12	0.78
Foil	....	....	....	....
Goil	....	....	....	....
Fsed	63.0	6.6	6.6	63.0
Gsed	0.80	1.7	1.7	0.80
K_1	1.9	4.00	4.0	1.9
K_2	6.6	0.98	0.98	6.6
PROBE 2				
Fvac	2.1	0.77	0.76	2.1
Gvac	0.06	0.13	0.13	0.06
Foil	....	....	....	....
Goil	....	....	....	....
Fsed	17.0	37.0	38.0	17.0
K_1	23.0	7.4	7.4	23.0
K_2	7.1	2.4	2.5	7.10
	0.88	2.1	2.1	0.88

Table IX. Standard Deviation and Variation of Dynamic Rigidity Parameters. (Cont.)

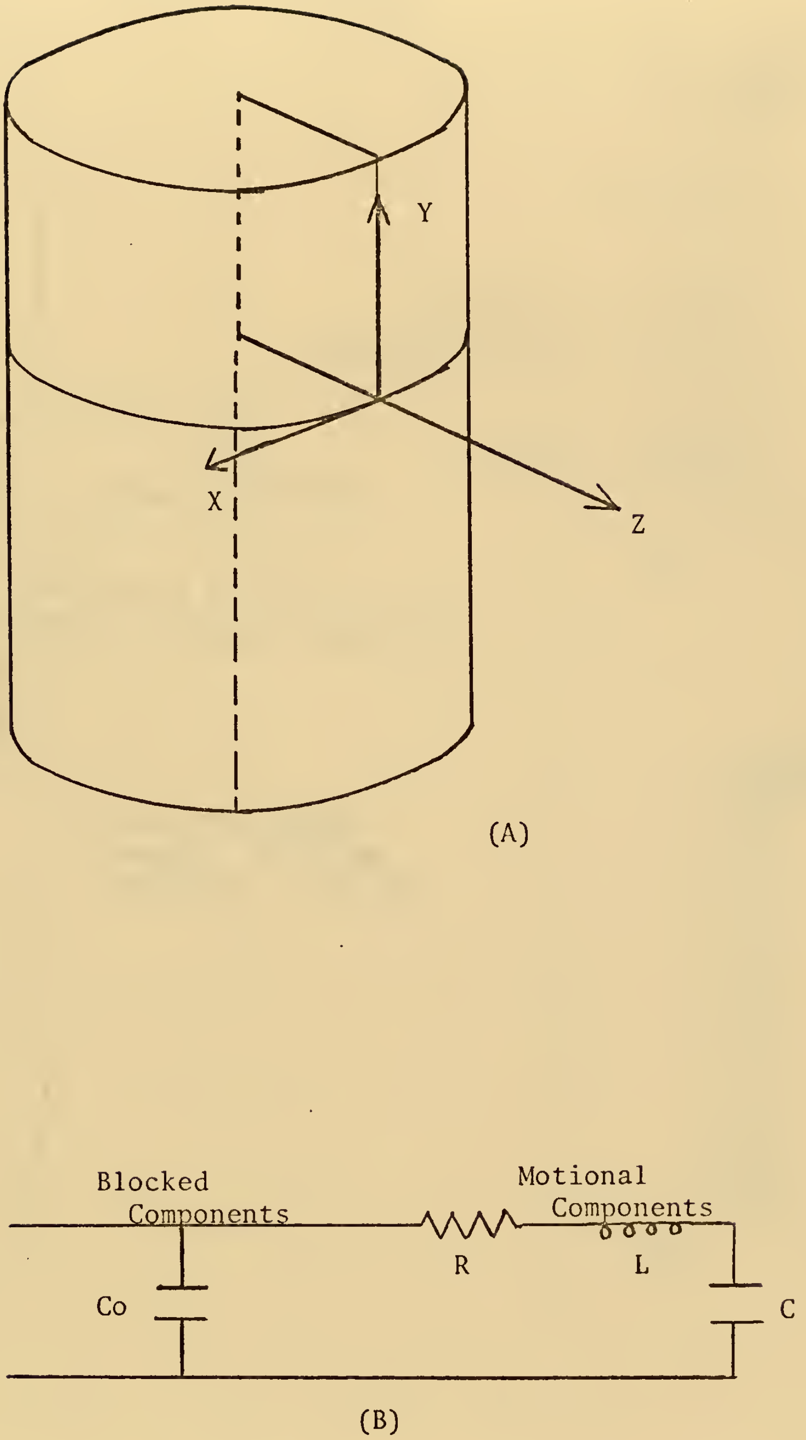

Figure 1. (A) Coordinates for Shear Wave Propagation
(B) Equivalent Electrical Circuit of Rod-Transducer System.

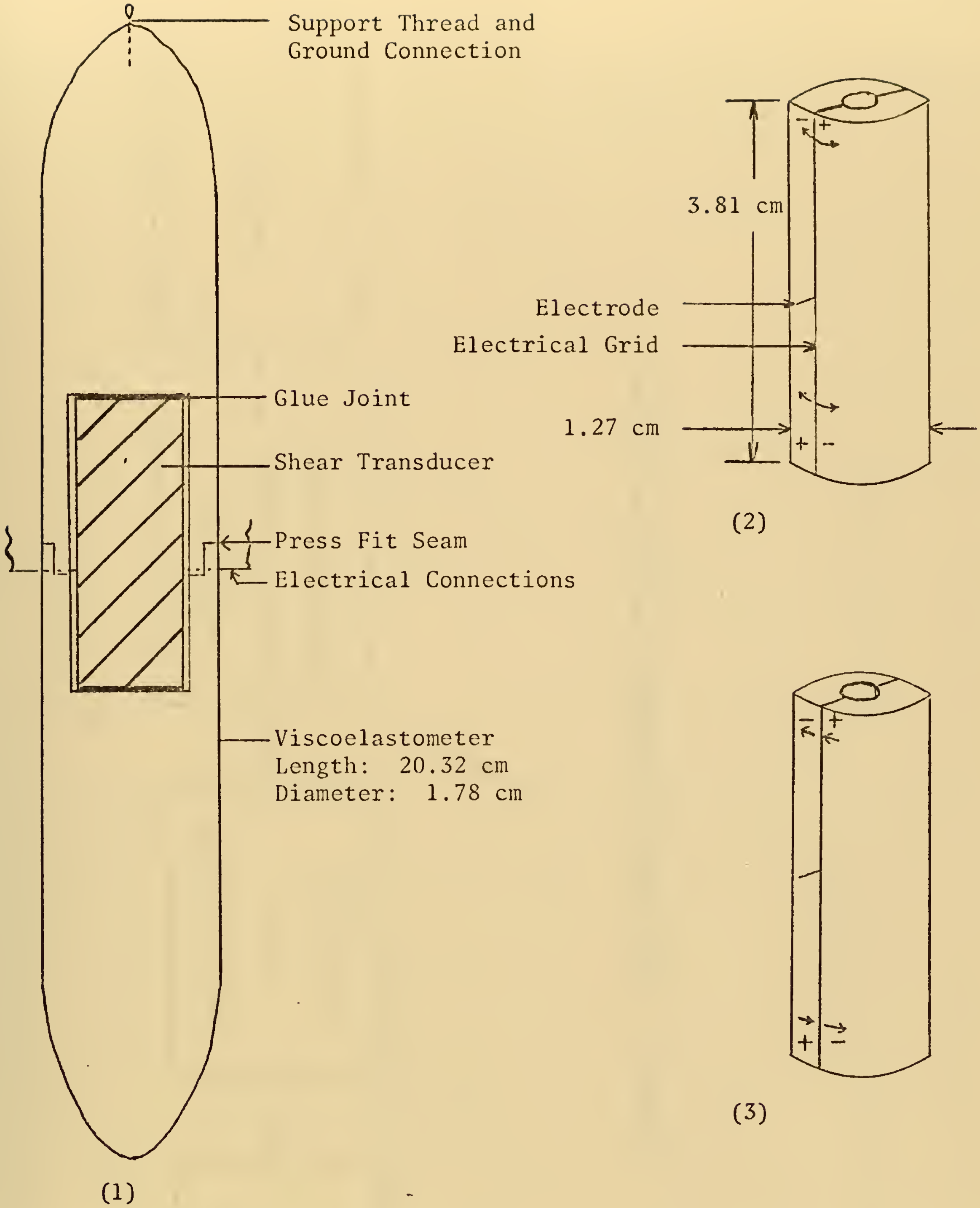

Figure 2. (1) Cut-Away View of Viscoelastometer
(2) Polarity of Shear Transducer, Field Direction
(3) Shear Stress Directions.

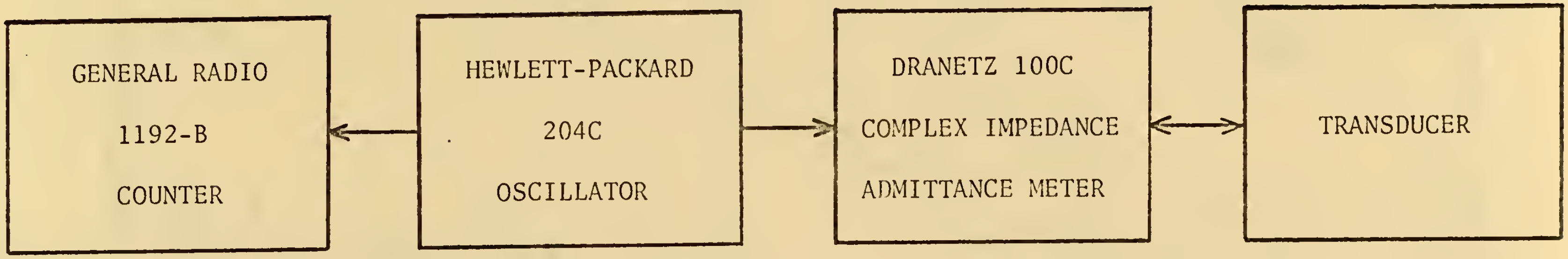

Figure 3. Block Diagram of Equipment for Resonance Method.

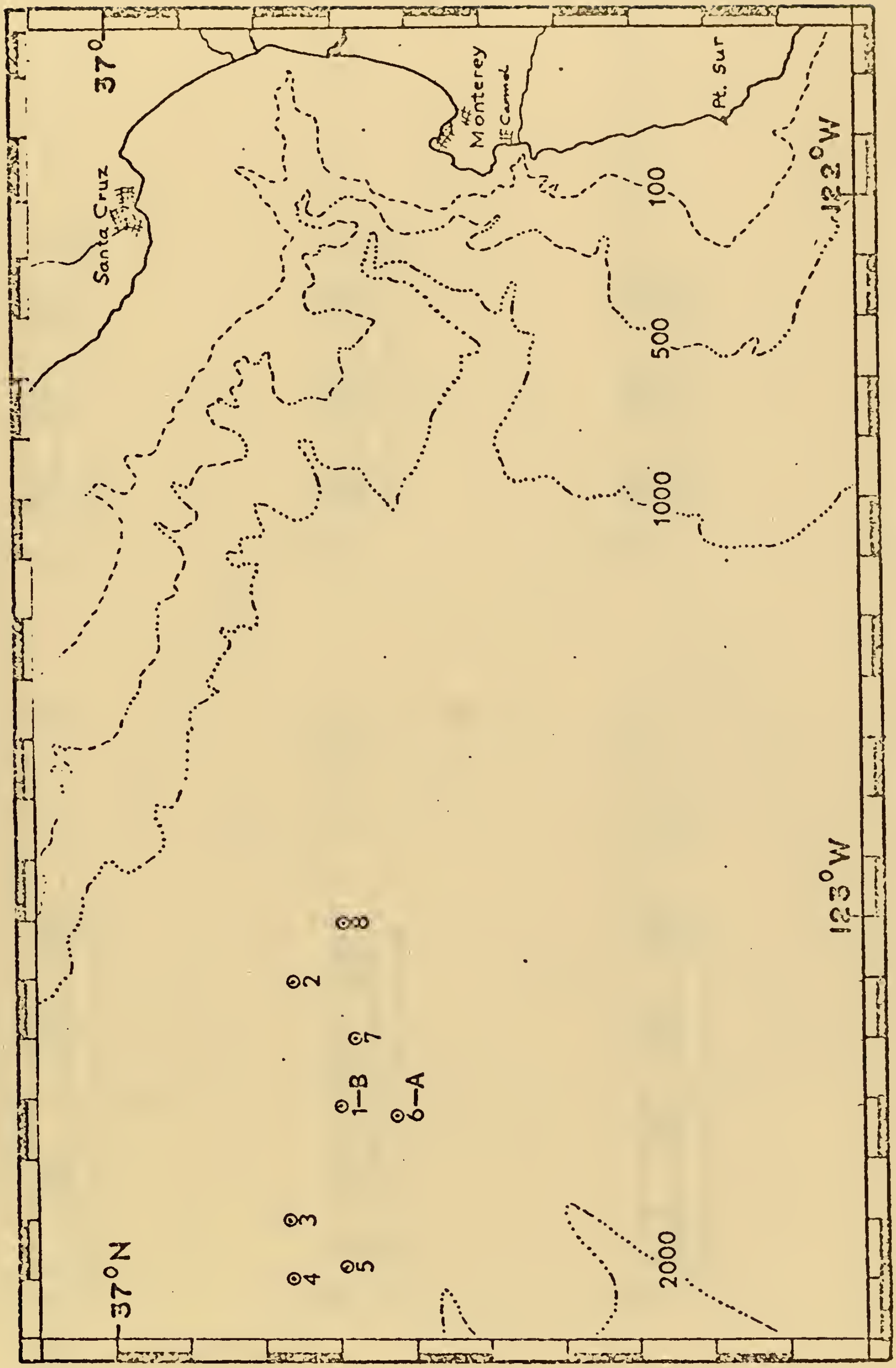

Figure 4. Coring Station Locations
(Isobaths in Fathoms).

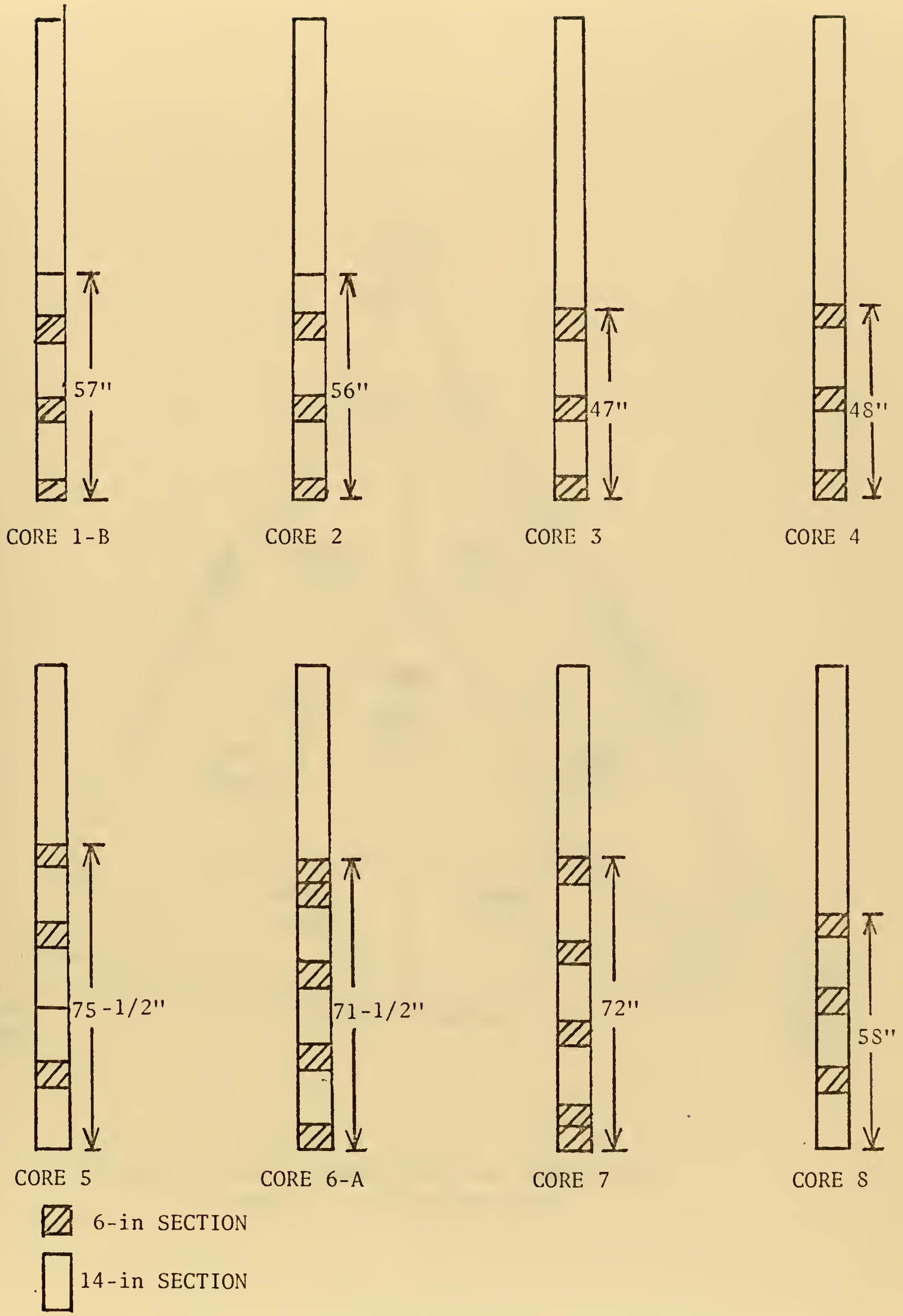

Figure 5. Sectioning of Cores.

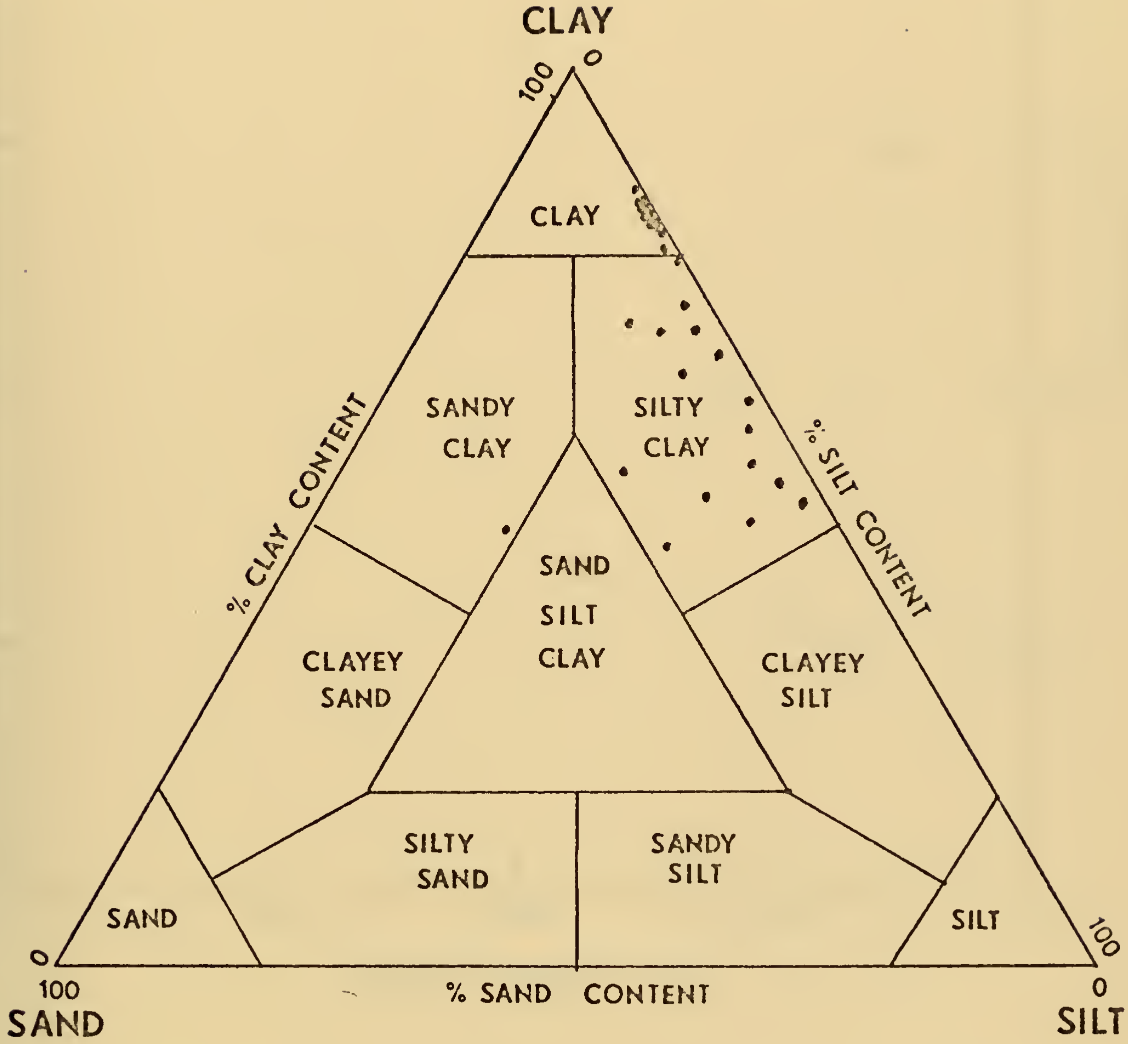

Figure 6. Plot of Sand/Silt/Clay Ratios for Each Core Section Analyzed.

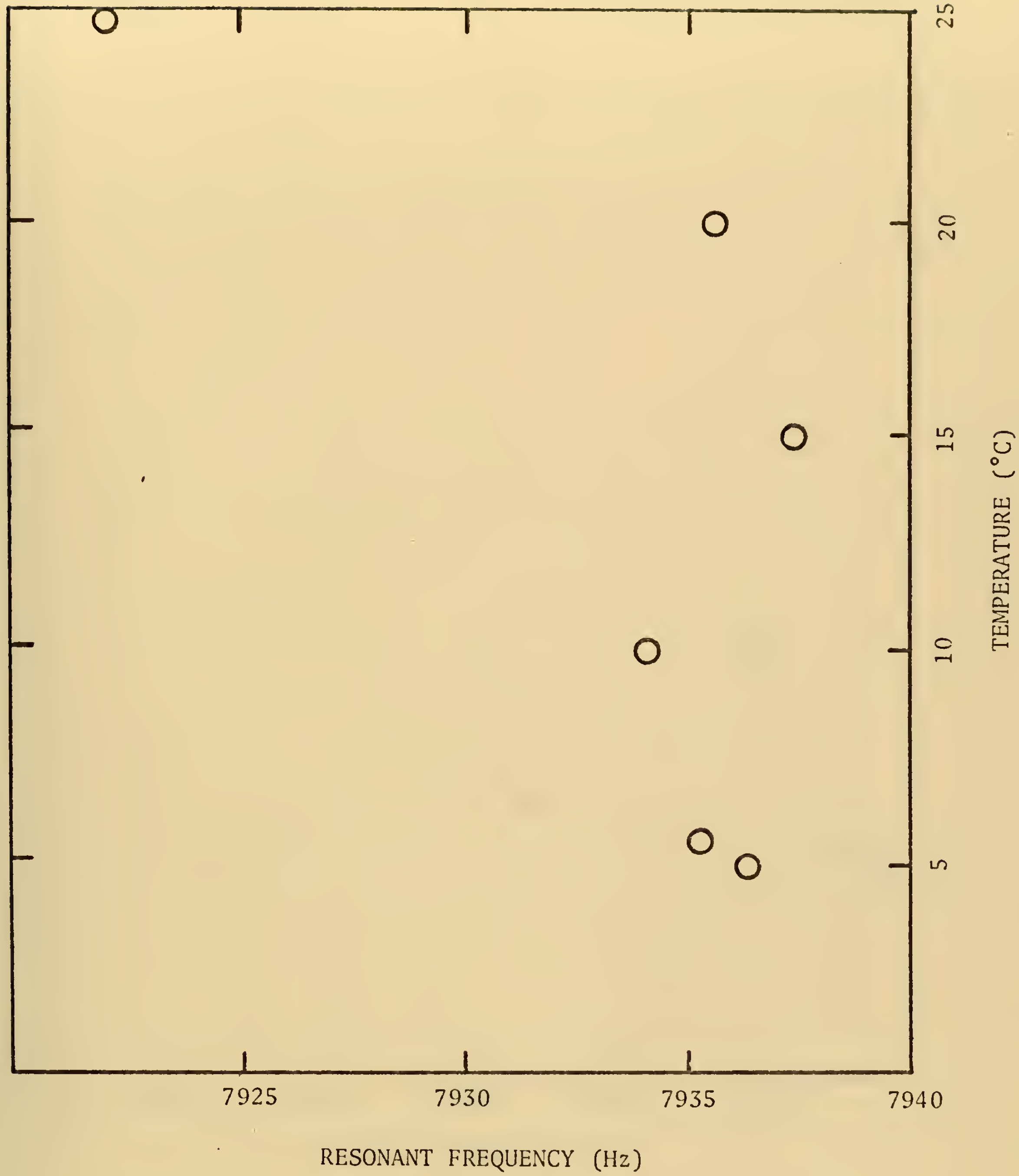

Figure 7. Resonant Frequency as a Function of Temperature Probe 1, Mode 1.

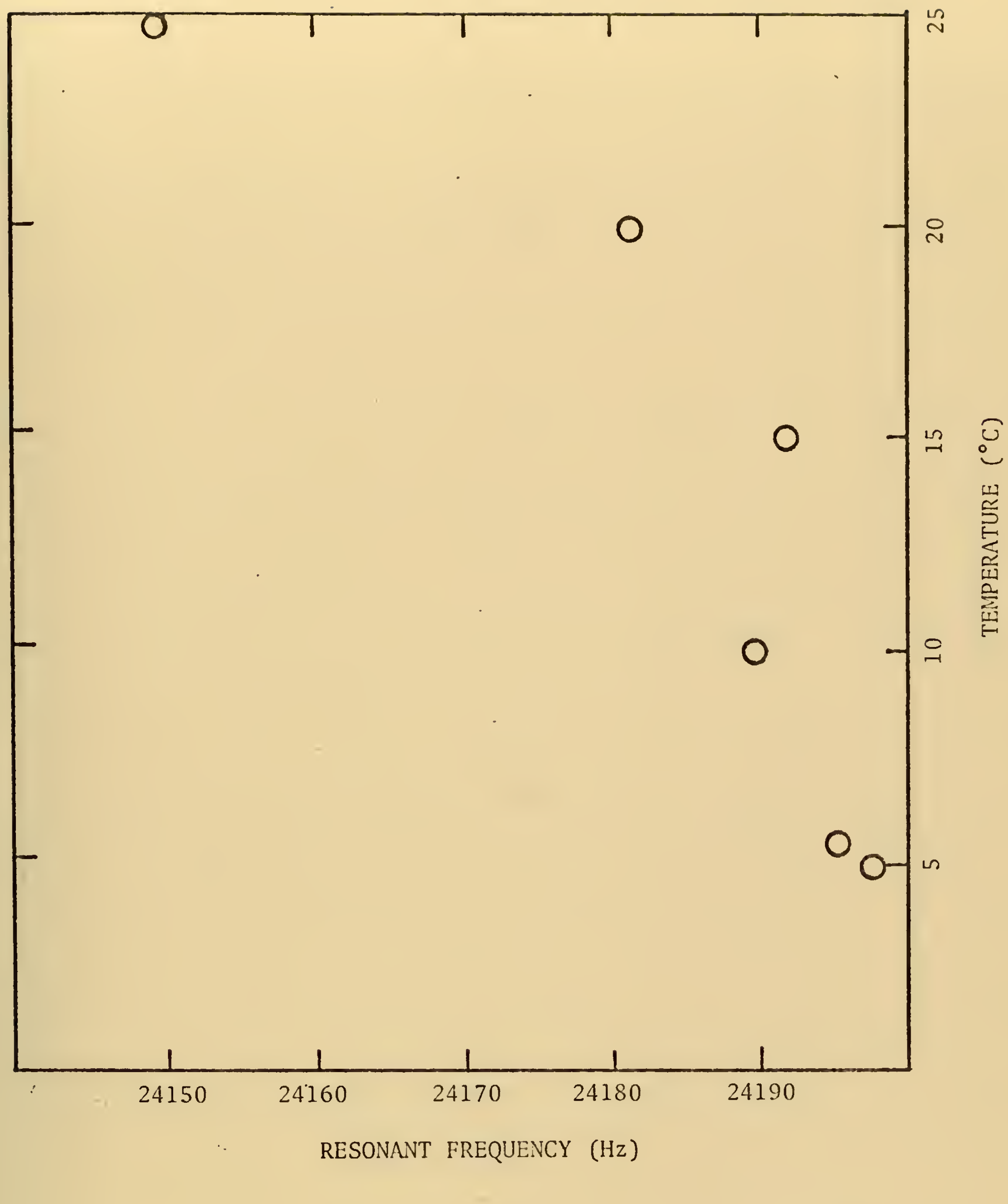

Figure 8. Resonant Frequency as a Function of Temperature Probe 1, Mode 2.

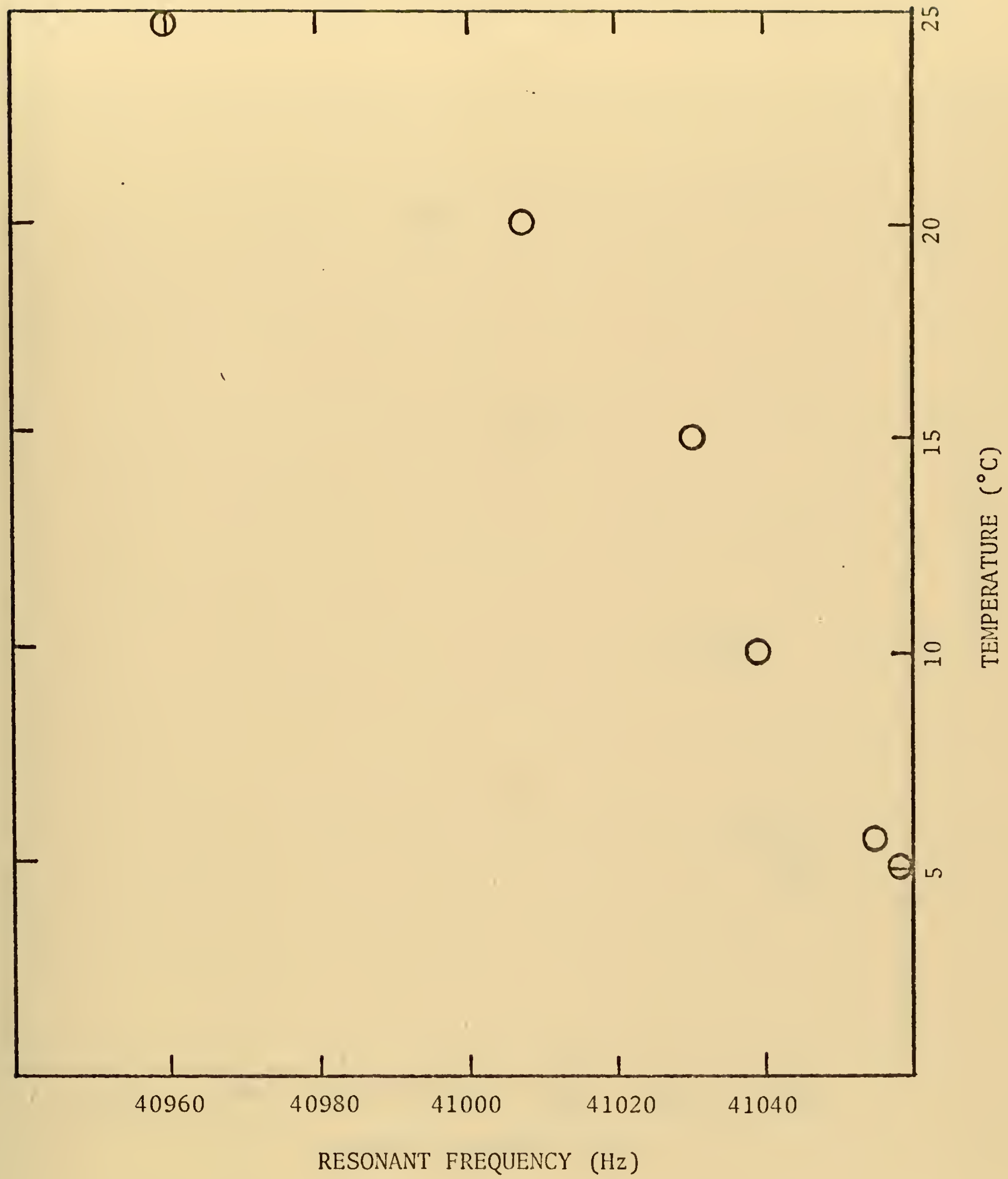

Figure 9. Resonant Frequency as a Function of Temperature Probe 1, Mode 3.

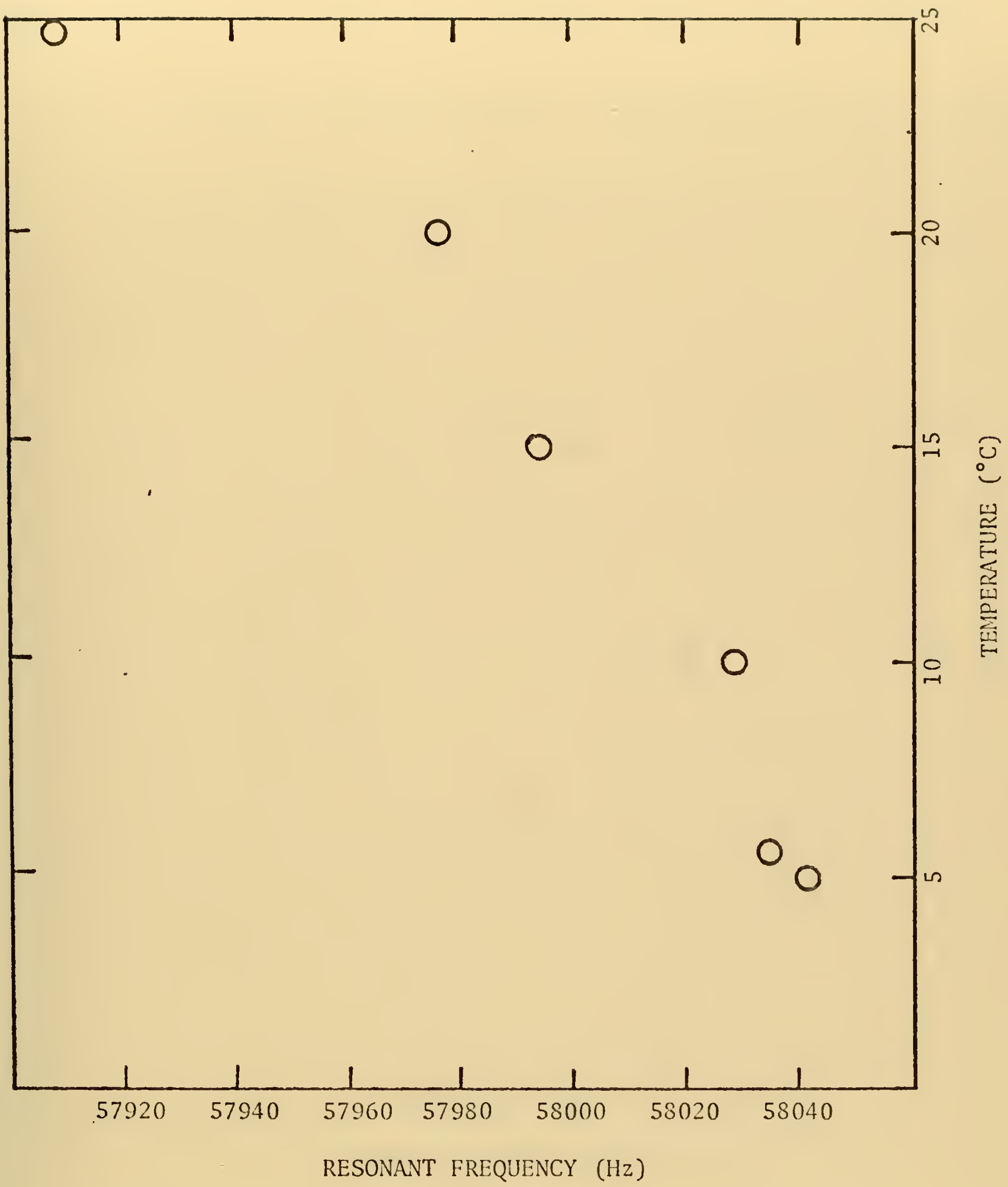

Figure 10. Resonant Frequency as a Function of Temperature Probe 1, Mode 4.

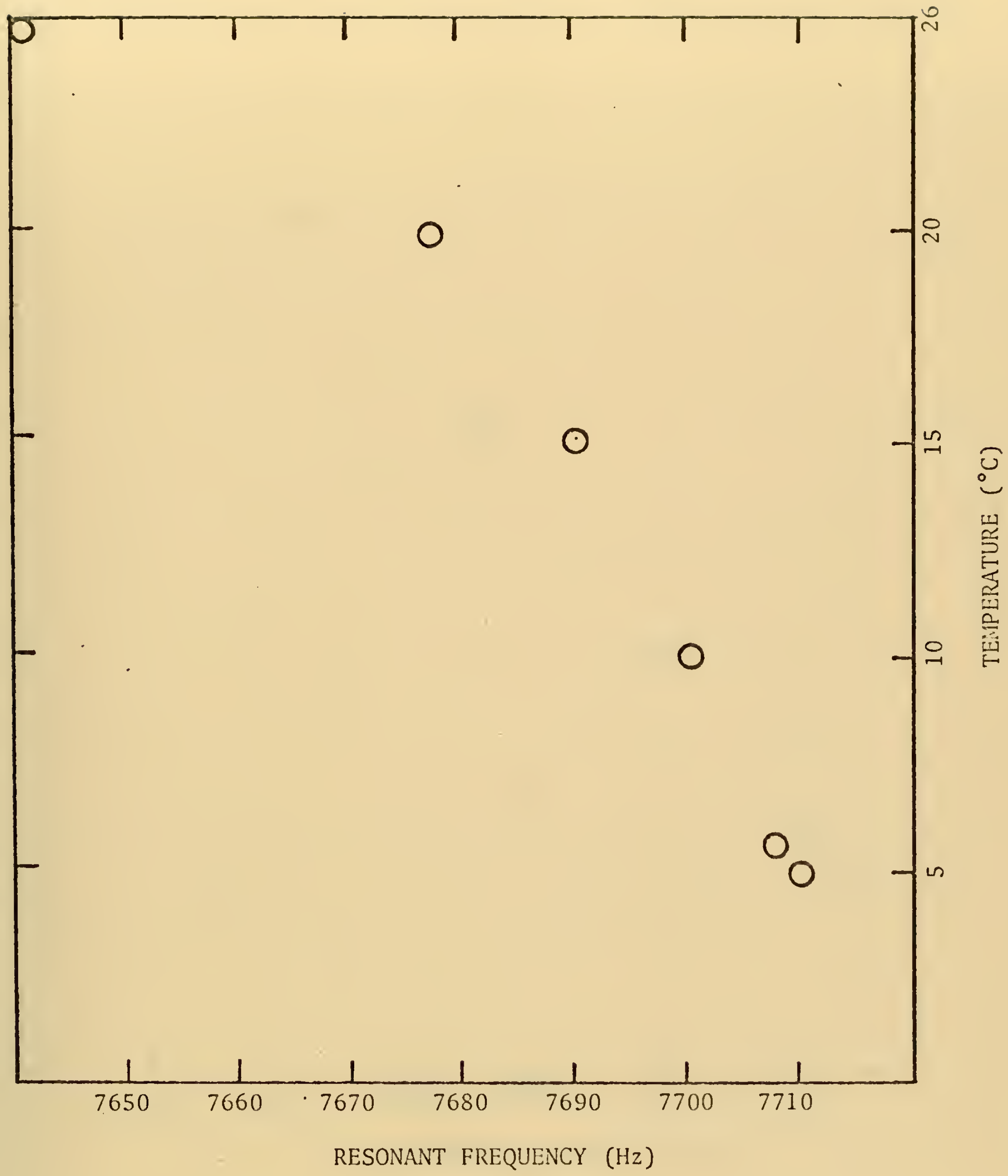

Figure 11. Resonant Frequency as a Function of Temperature Probe 2, Mode 1.

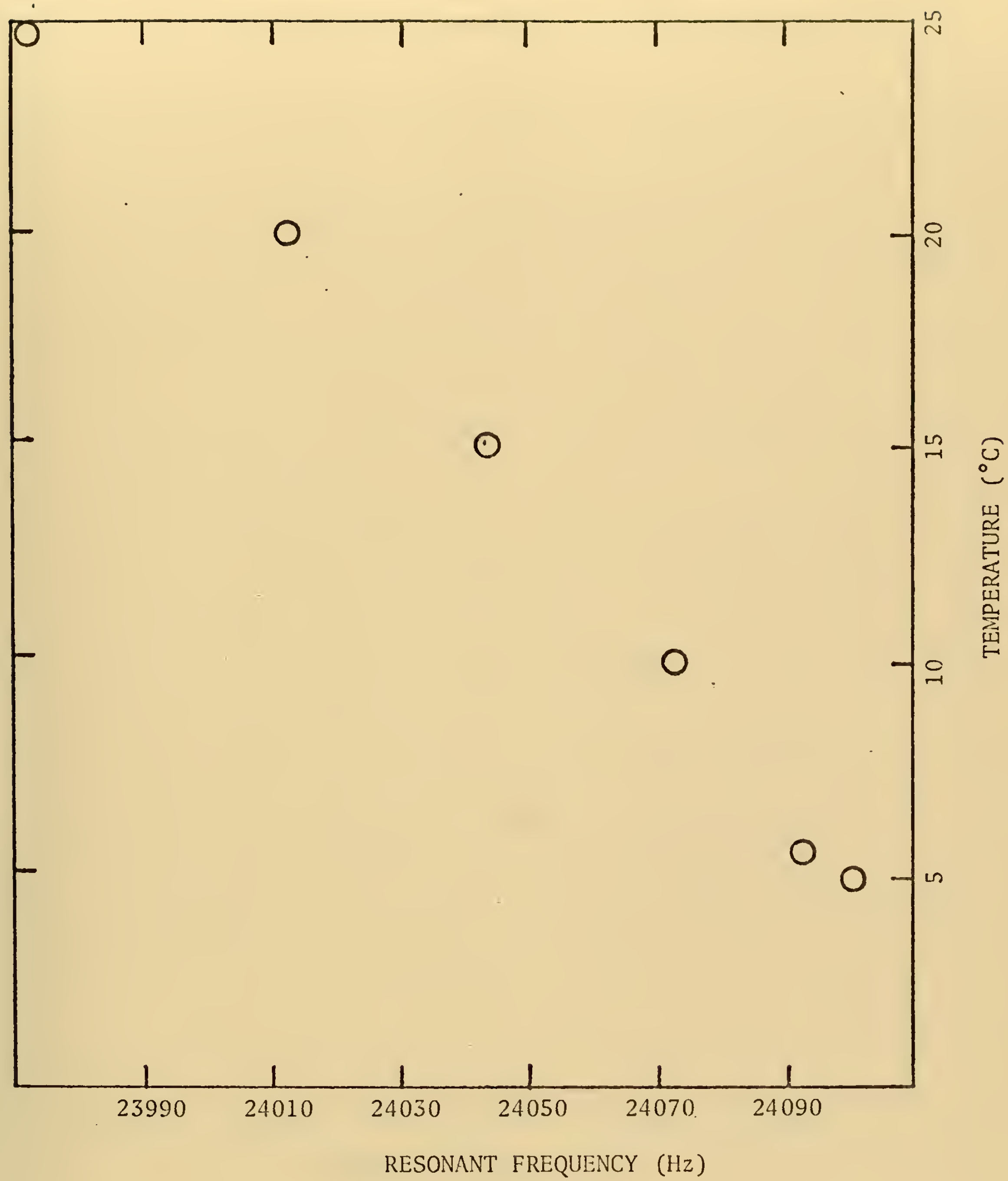

Figure 12. Resonant Frequency as a Function of Temperature Probe 2, Mode 2.

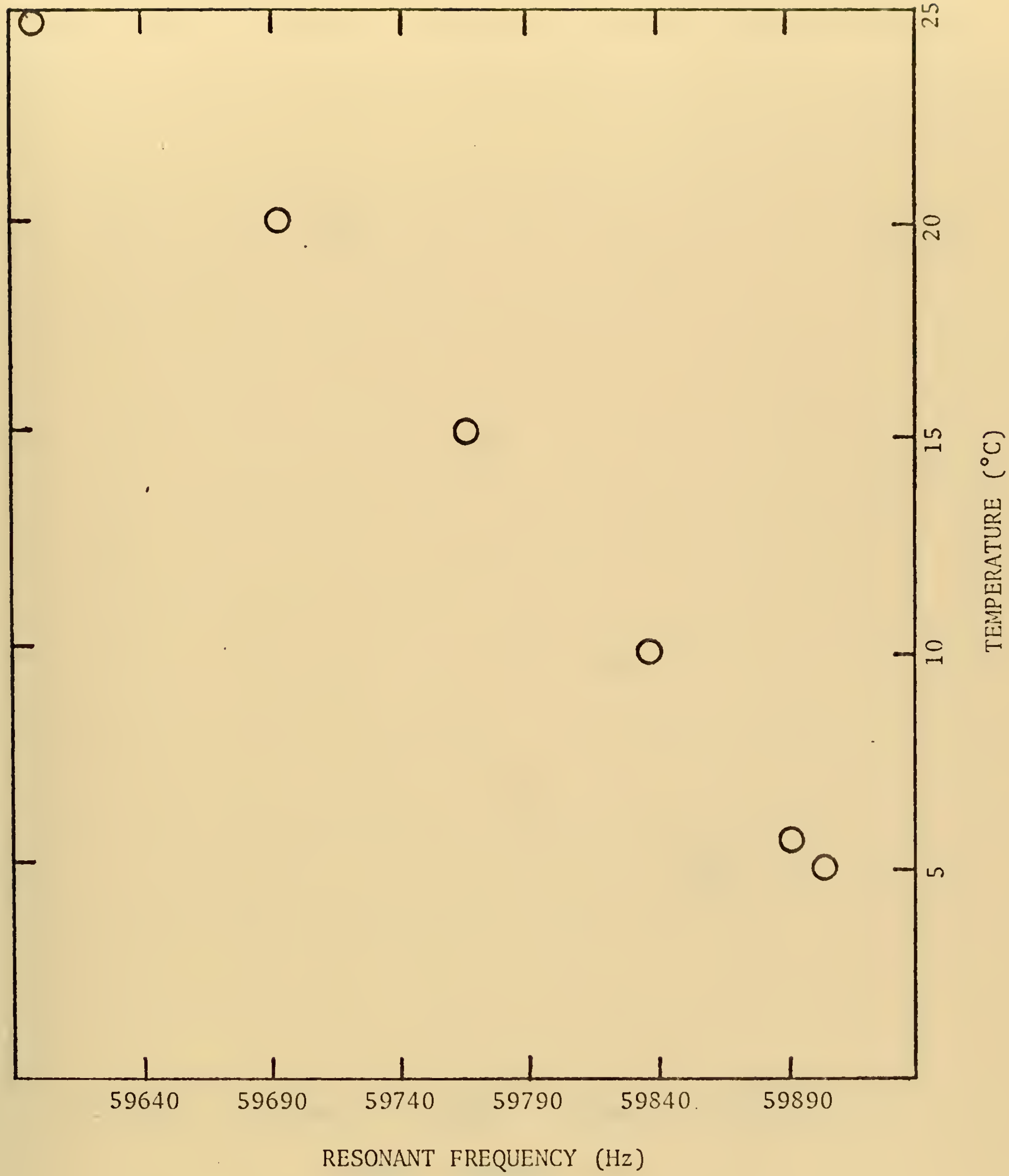

Figure 13. Resonant Frequency as a Function of Temperature Probe 2, Mode 3.

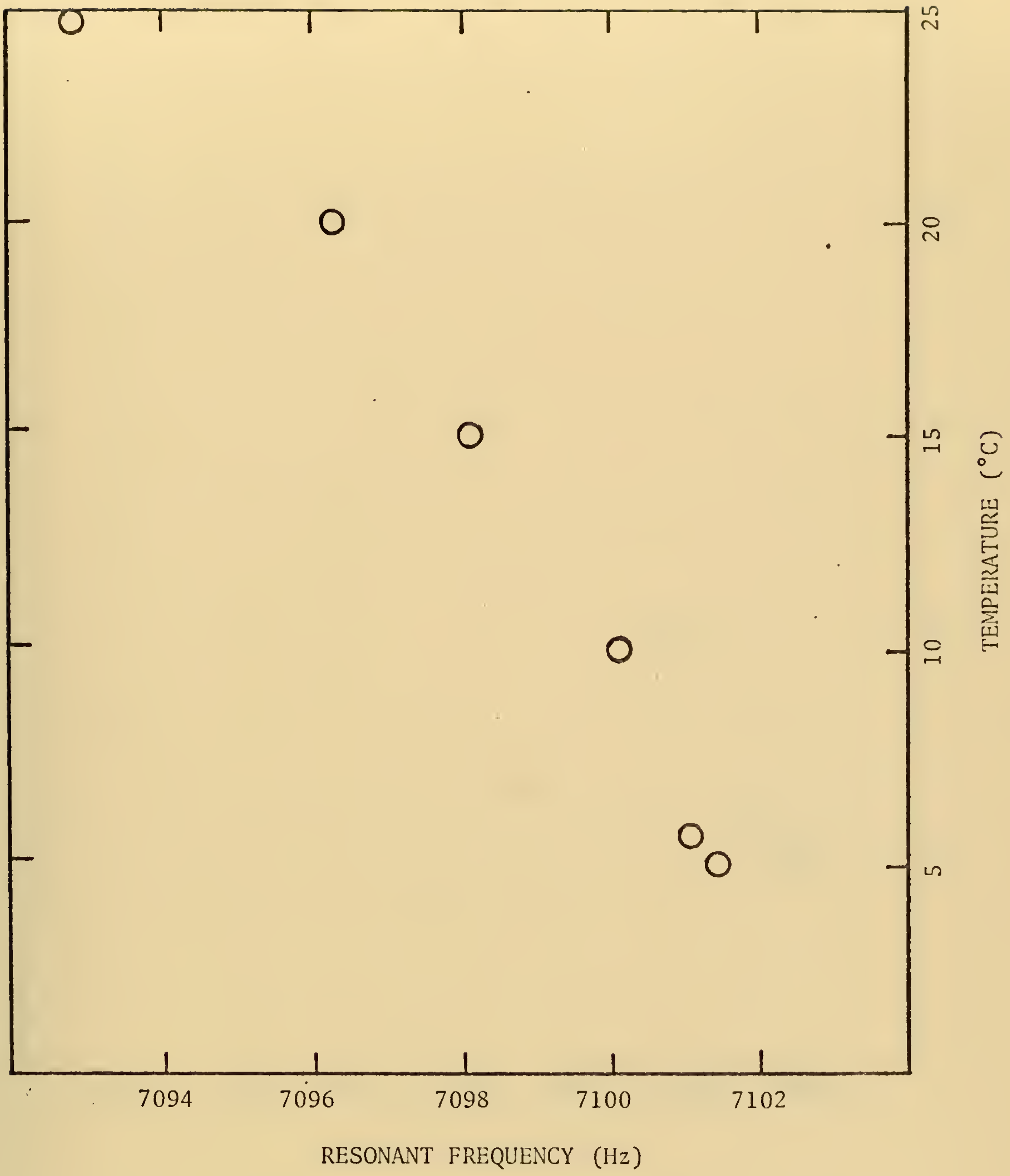

Figure 14. Resonant Frequency as a Function of Temperature Probe 4, Mode 1.

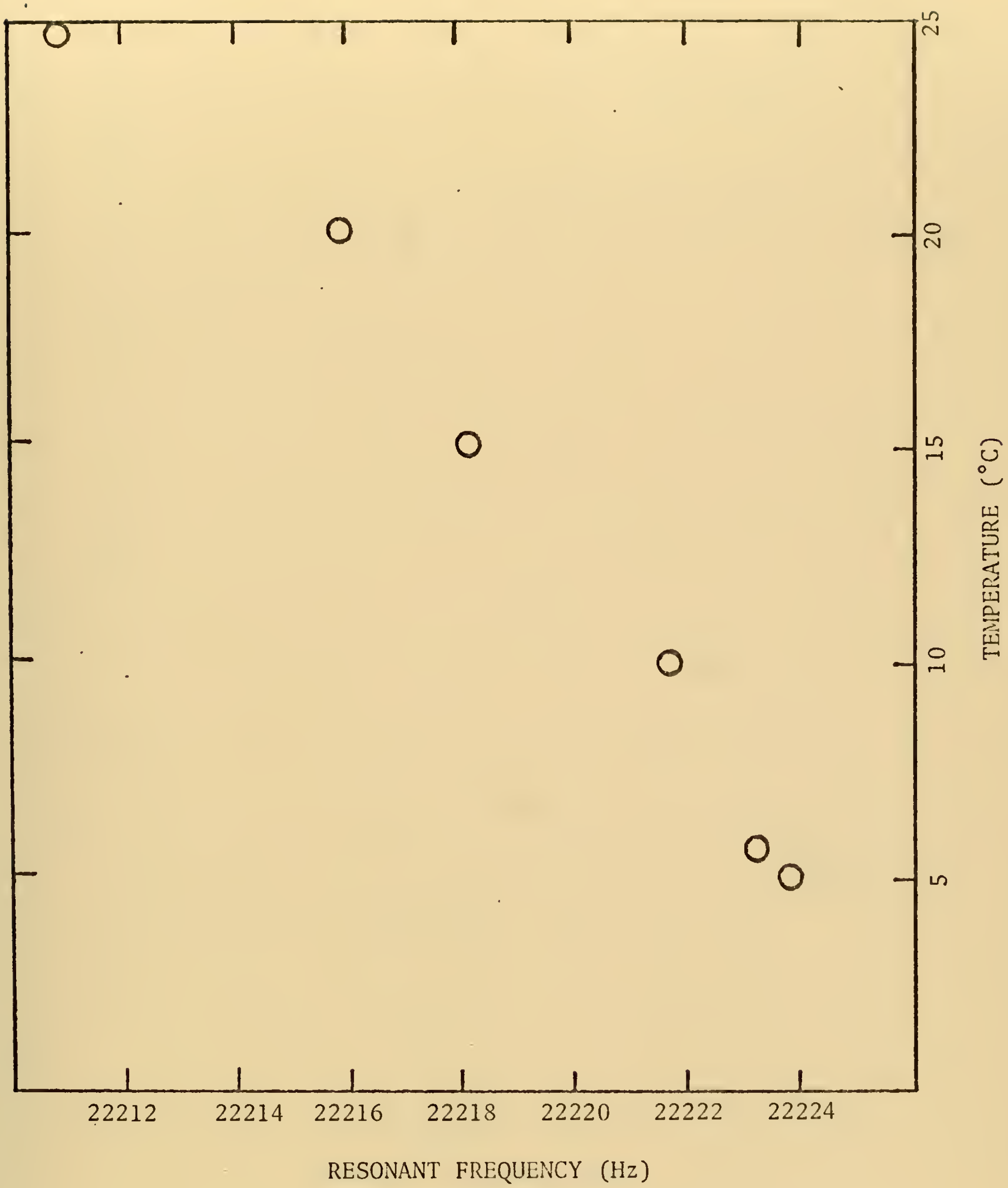

Figure 15. Resonant Frequency as a Function of Temperature Probe 4, Mode 2.

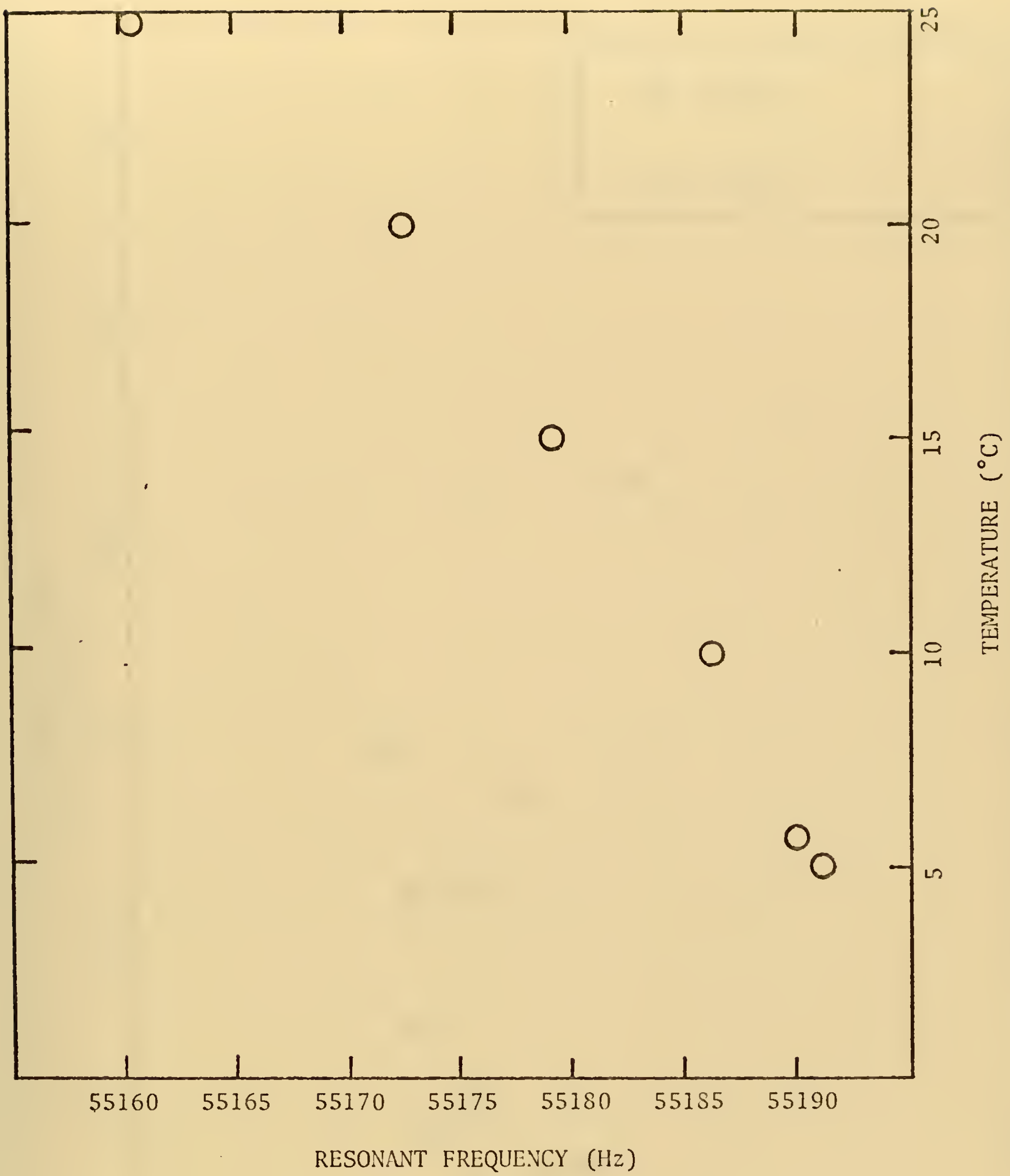

Figure 16. Resonant Frequency as a Function of Temperature Probe 4, Mode 3.

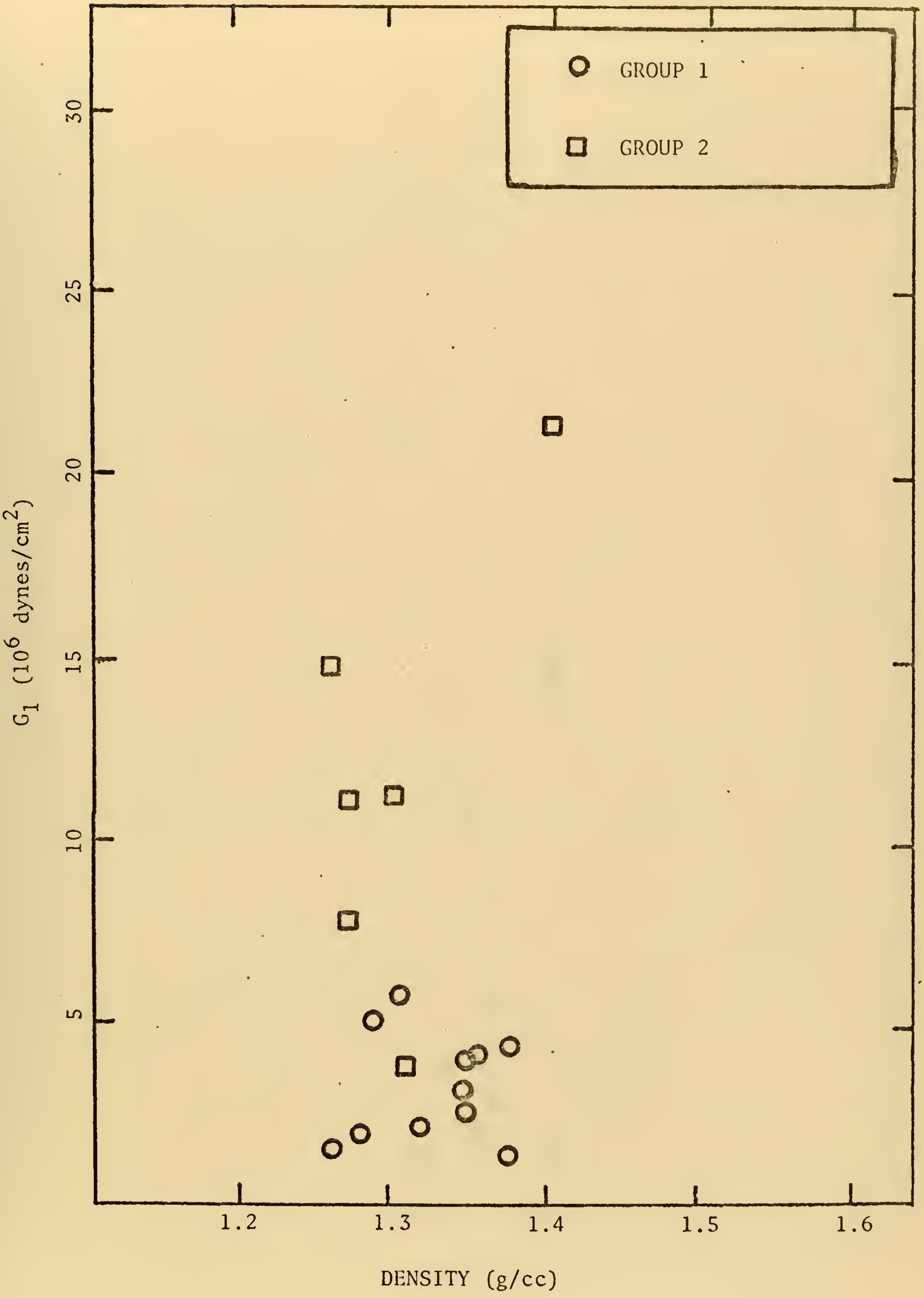

Figure 17. G_1 as a Function of Density.

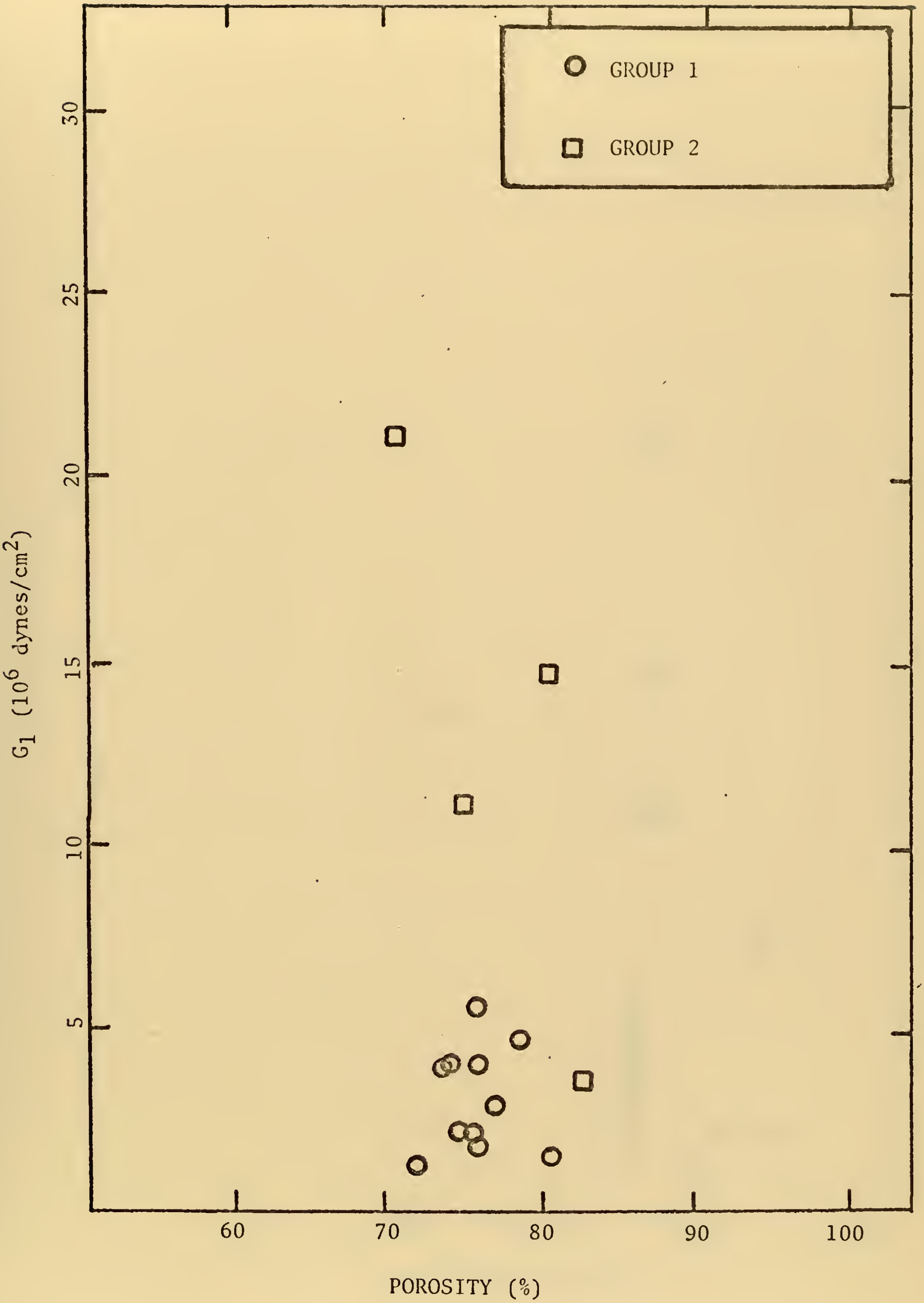

Figure 18. G_1 as a Function of Porosity.

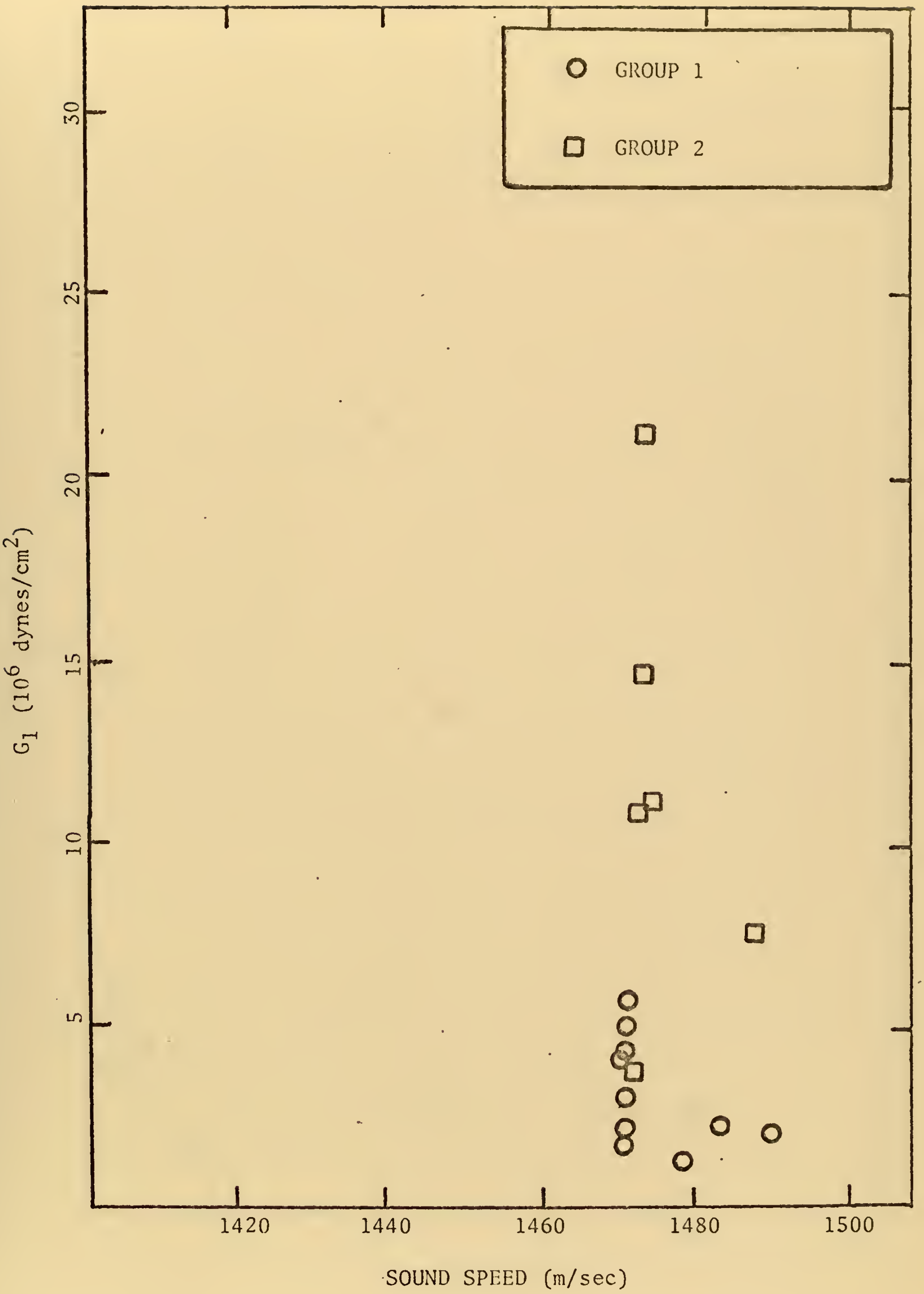

Figure 19. G_1 as a Function of Sound Speed.

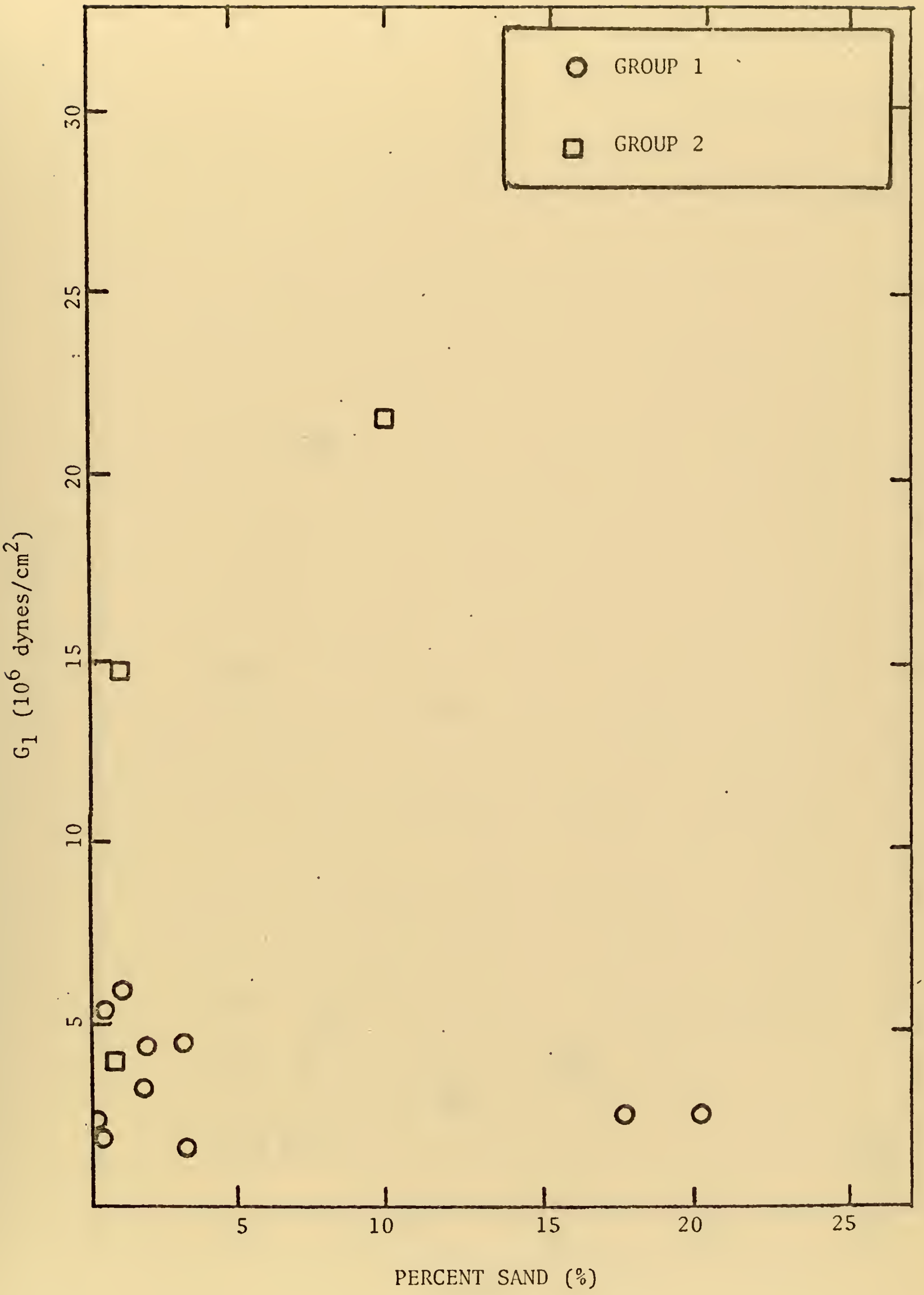

Figure 20. G_1 as a Function of Percent Sand.

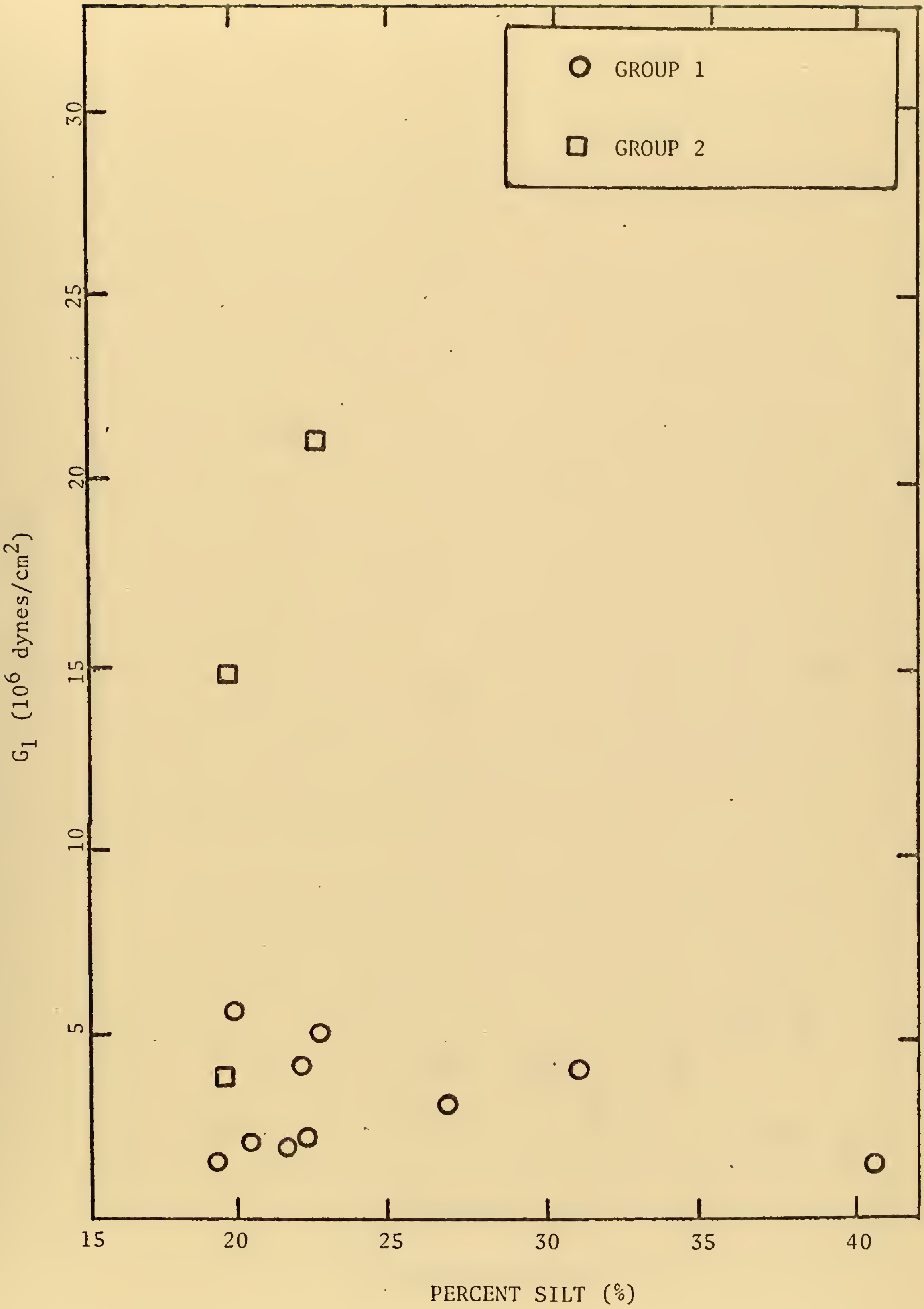

Figure 21. G_1 as a Function of Percent Silt.

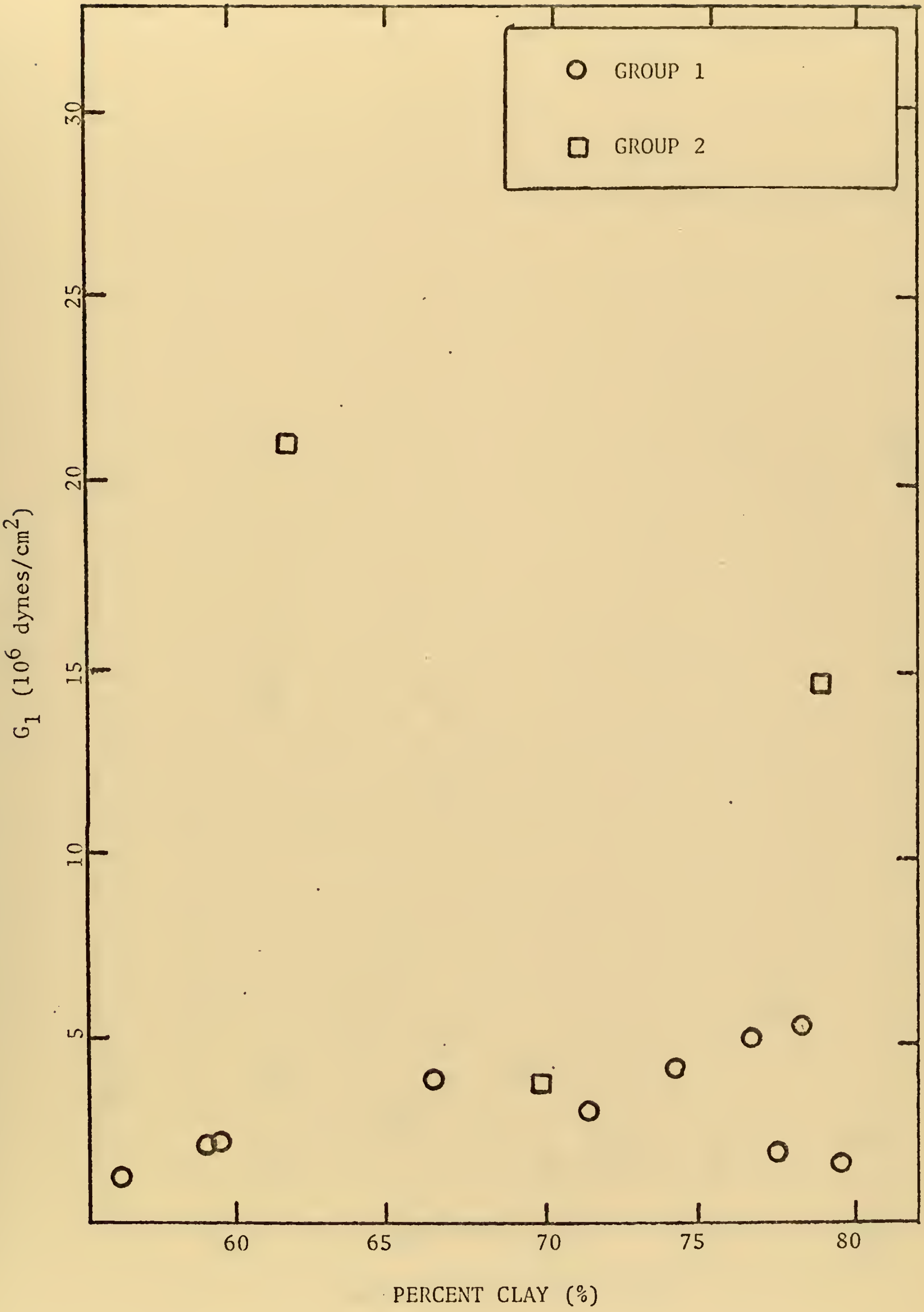

Figure 22. G_1 as a Function of Percent Clay.

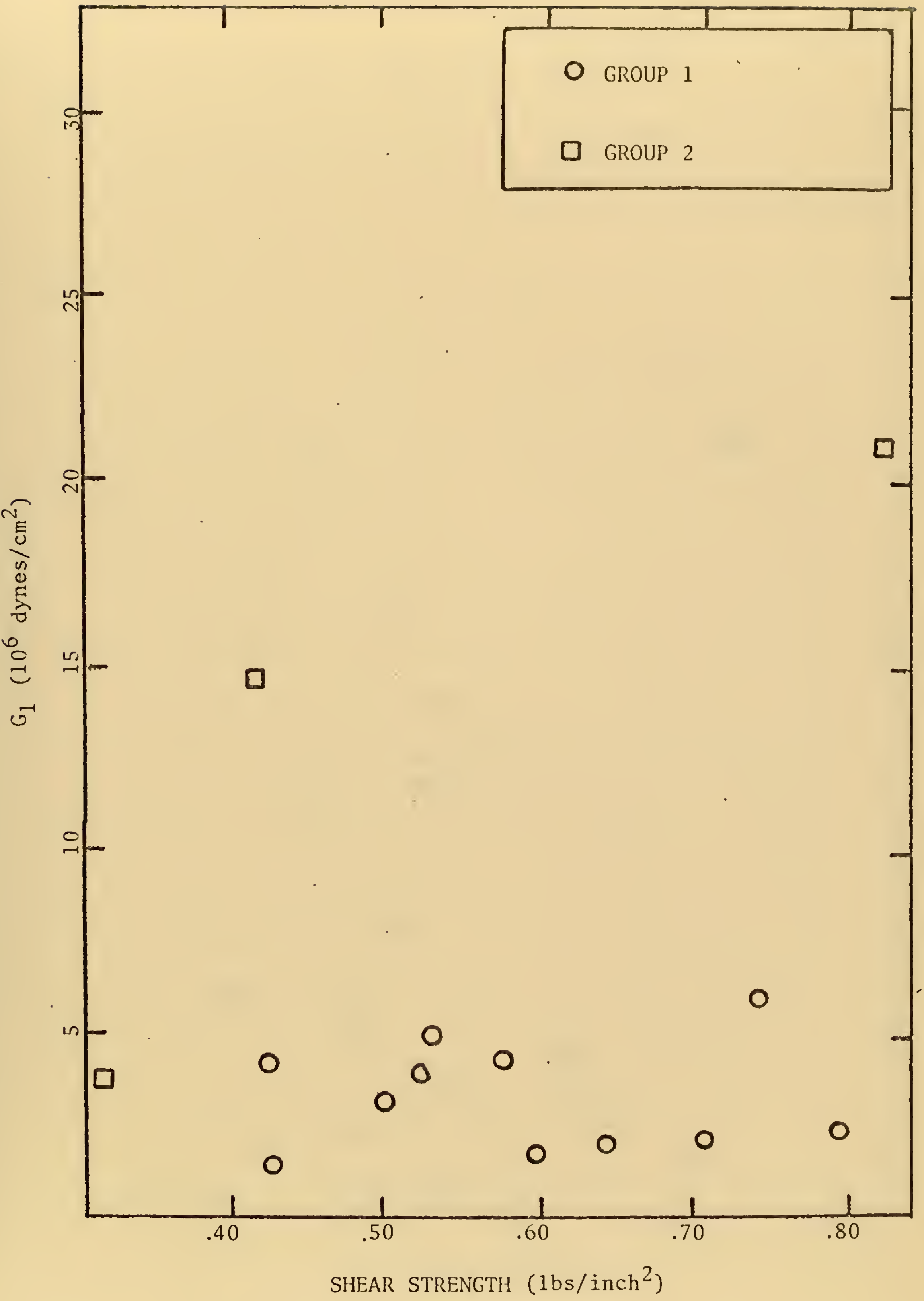

Figure 23. G_1 as a Function of Vane Shear Strength.

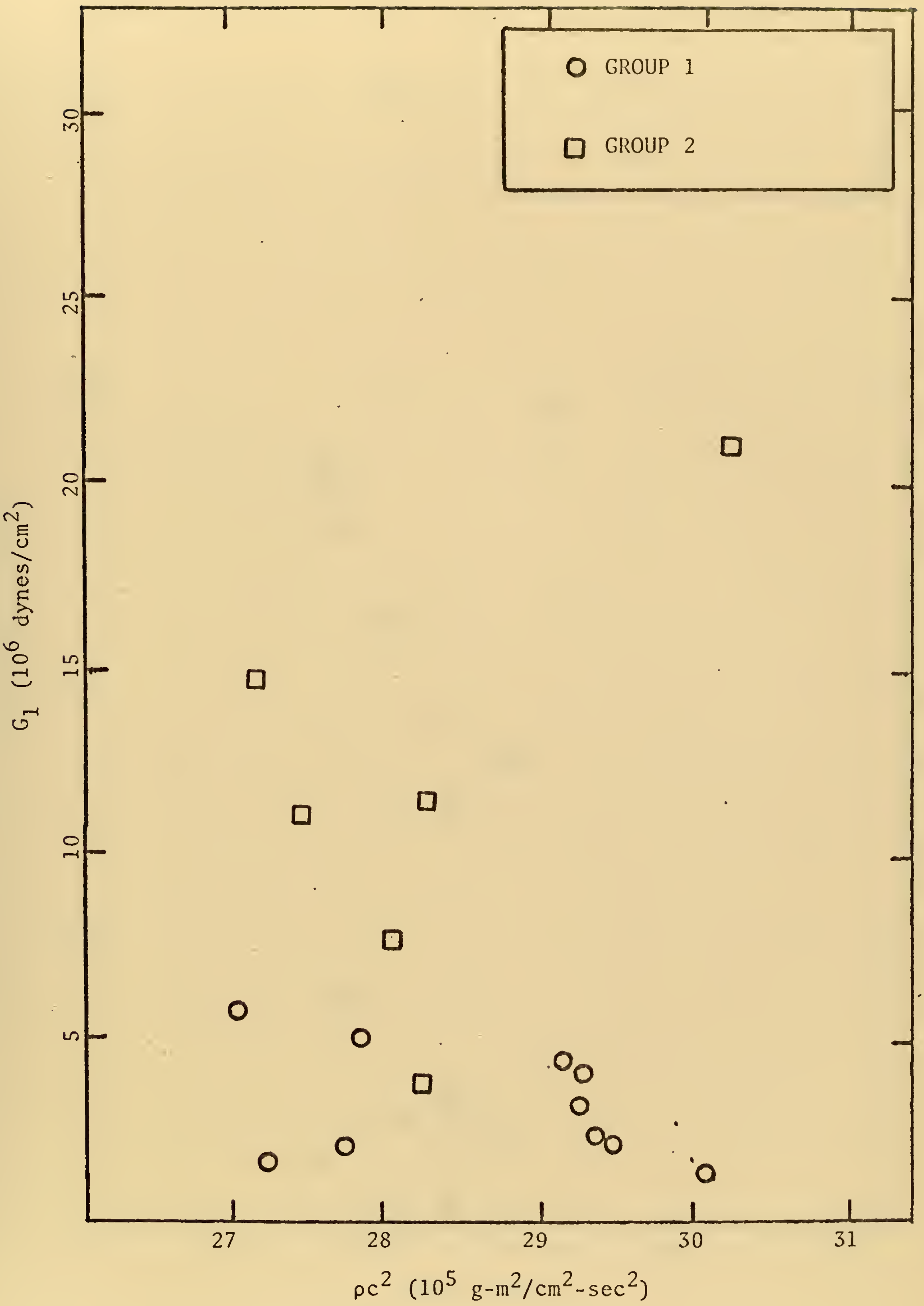

Figure 24. G_1 as a Function of the Product of Density and Sound Speed Squared.

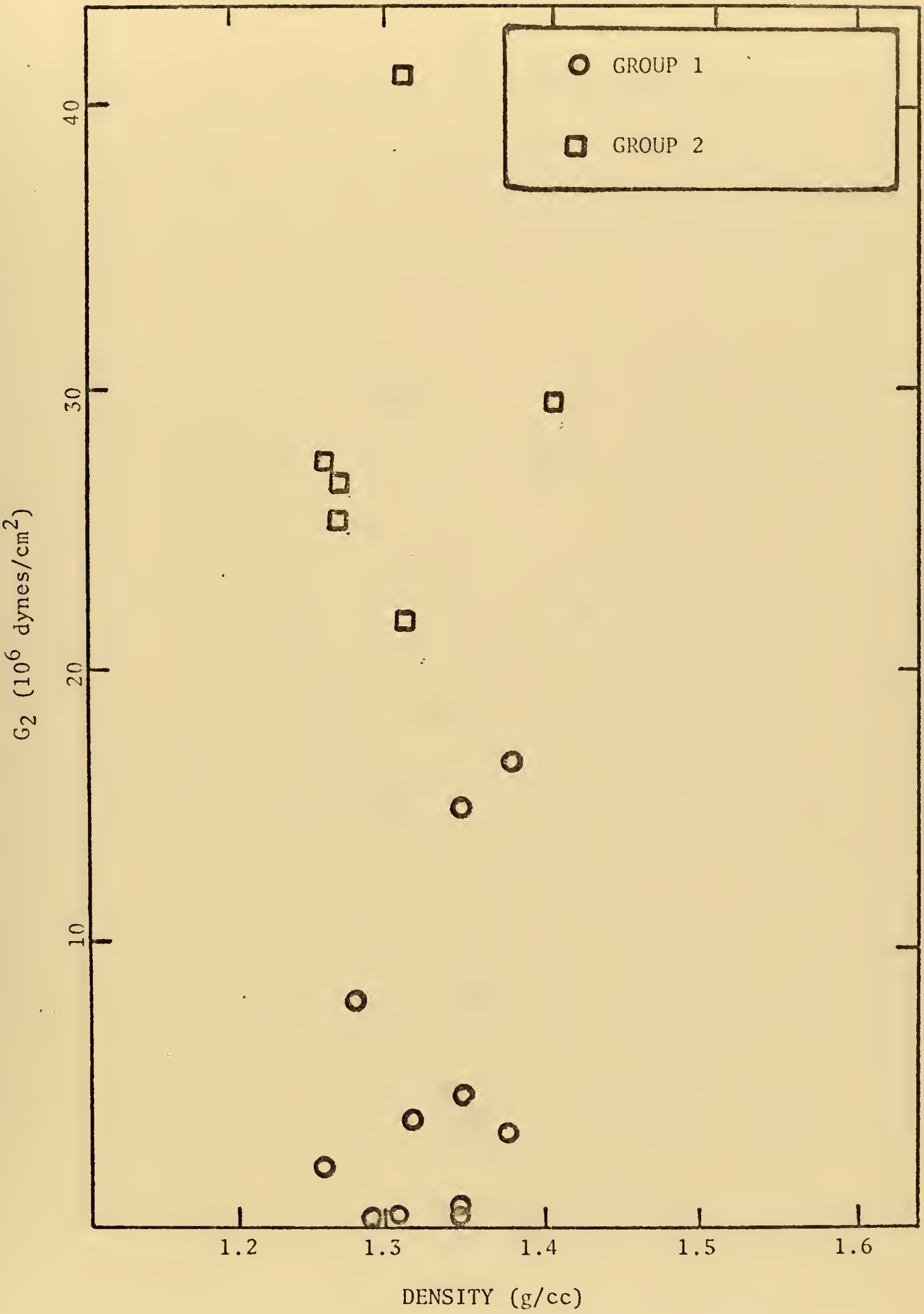

Figure 25. G_2 as a Function of Density.

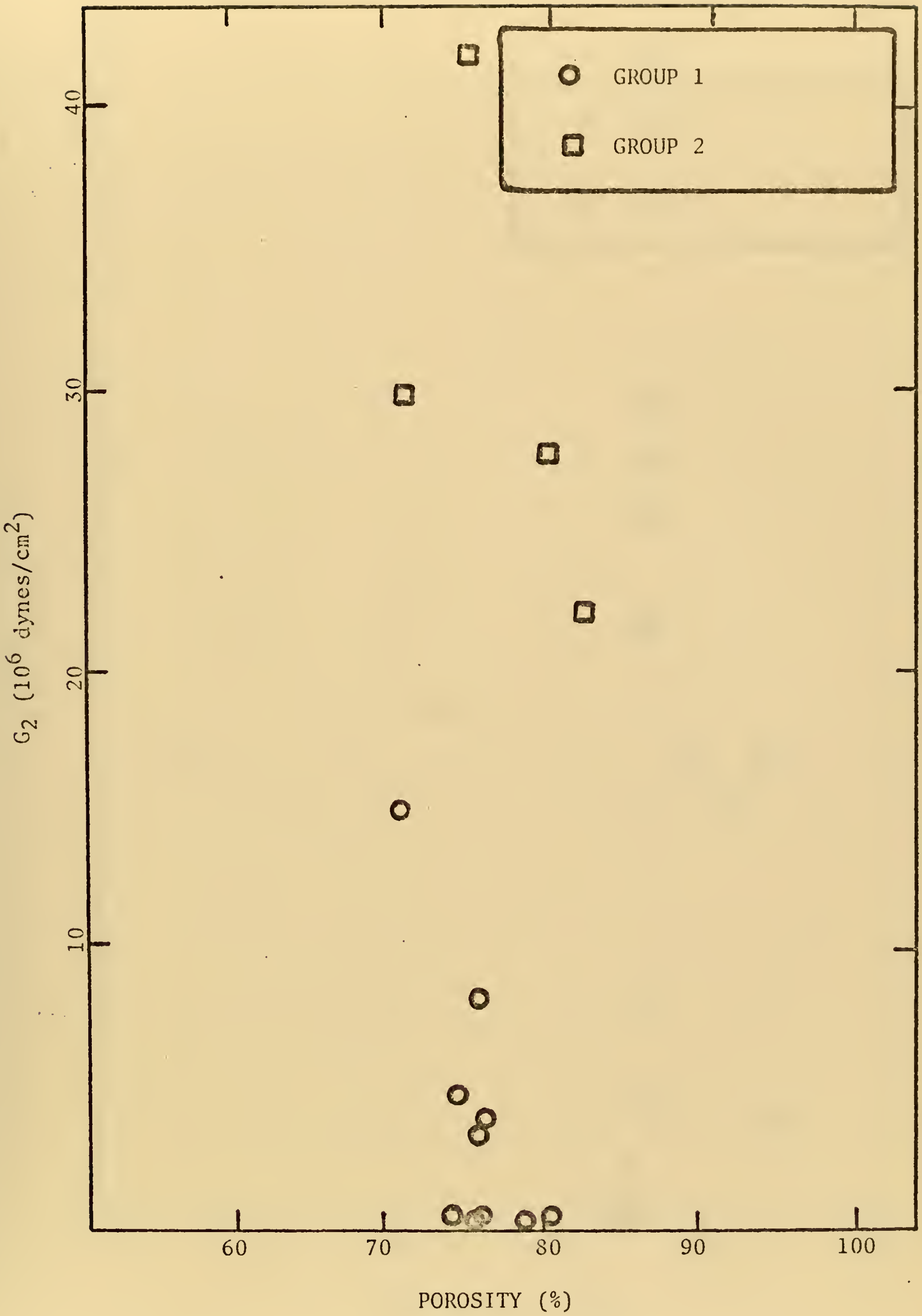

Figure 26. G_2 as a Function of Porosity.

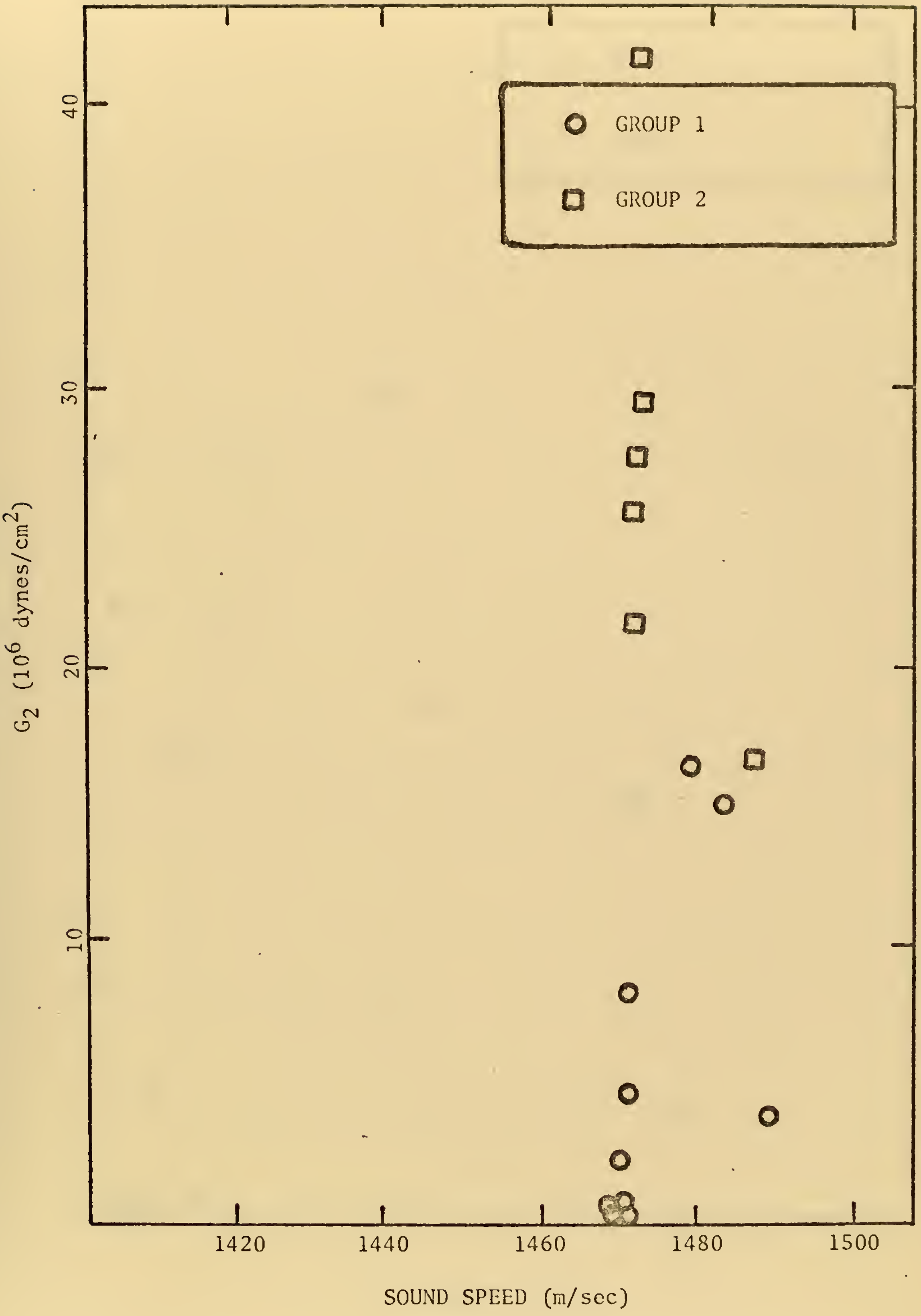

Figure 27. G_2 as a Function of Sound Speed.

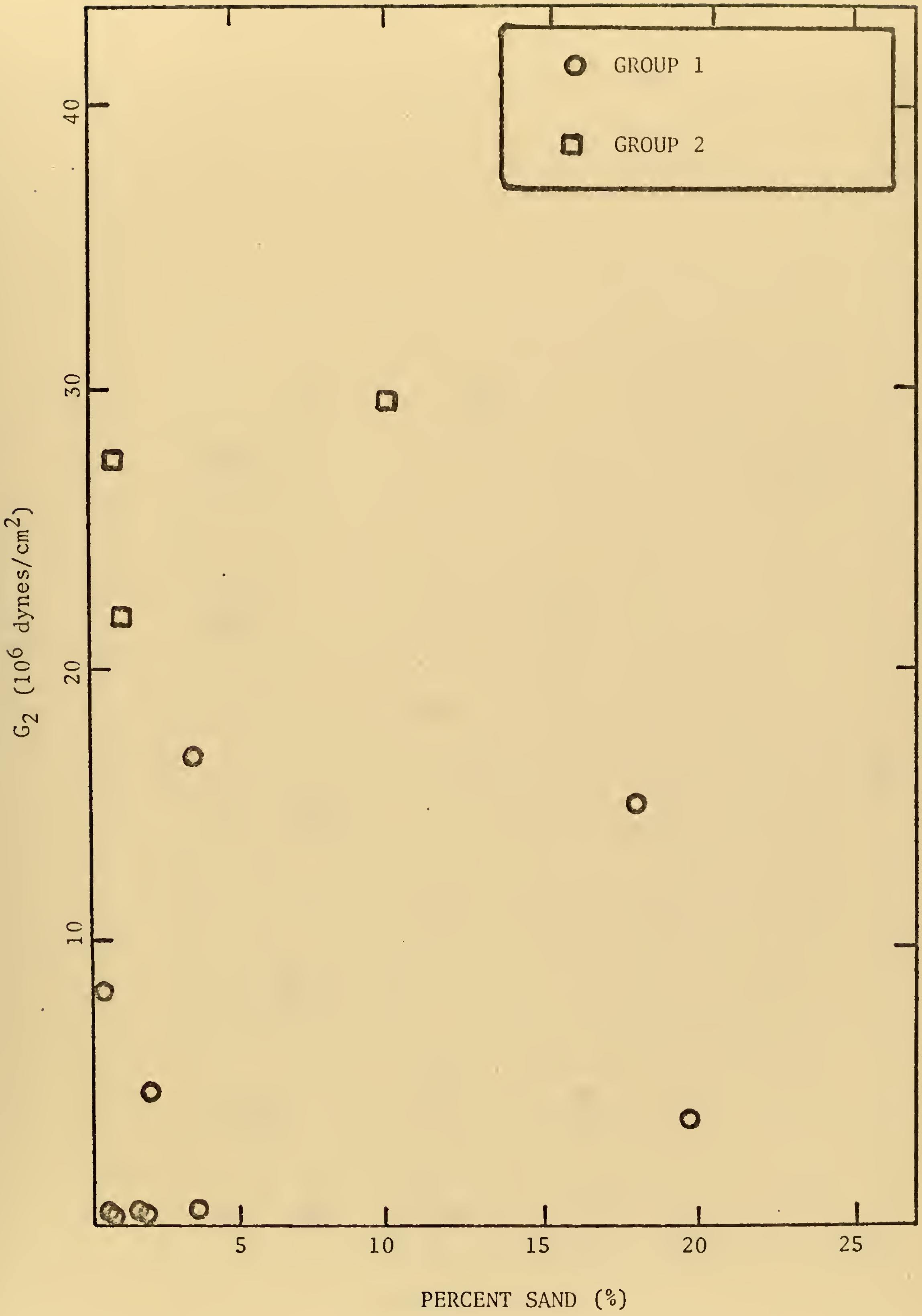

Figure 28. G_2 as a Function of Percent Sand.

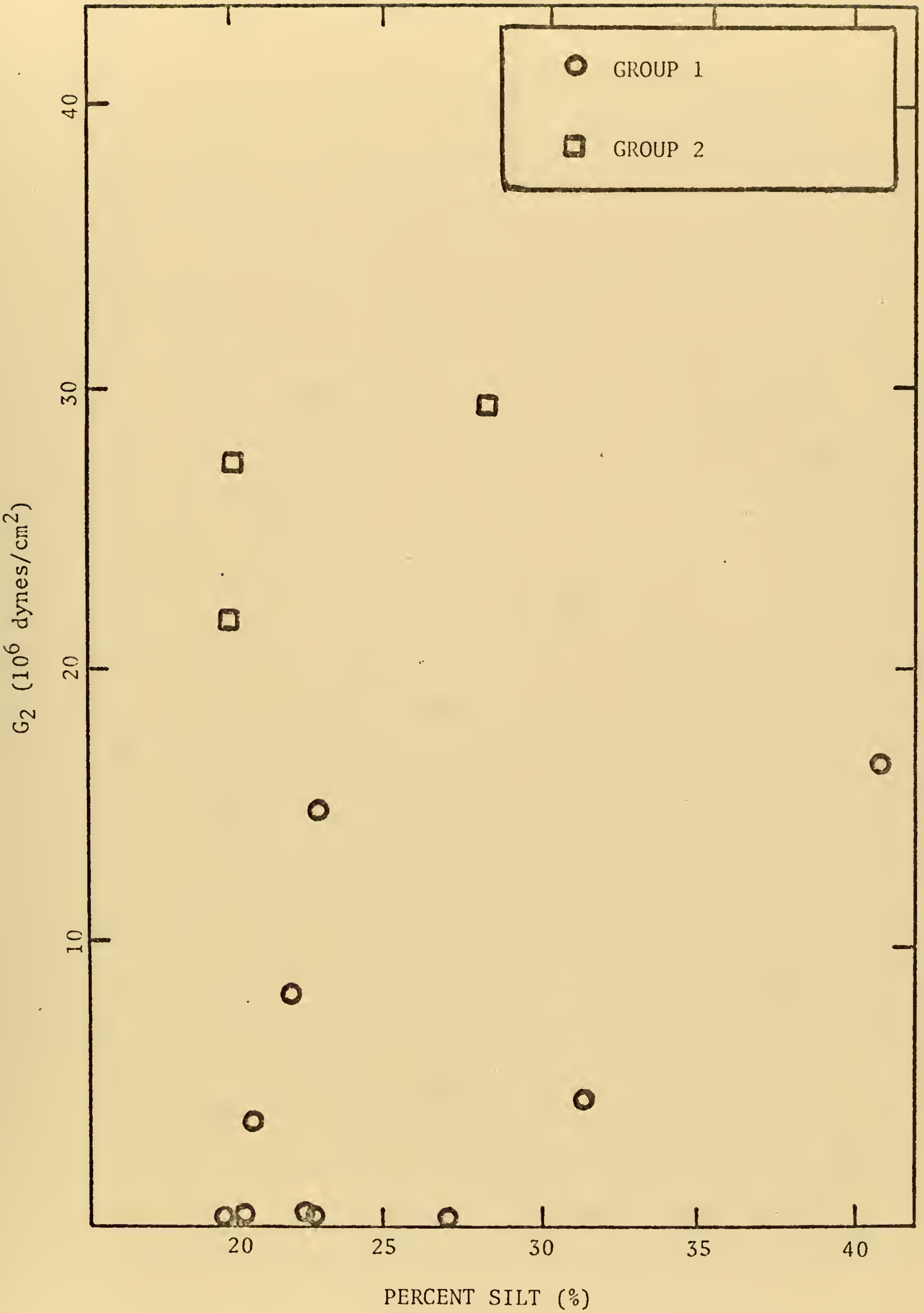

Figure 29. G_2 as a Function of Percent Silt.

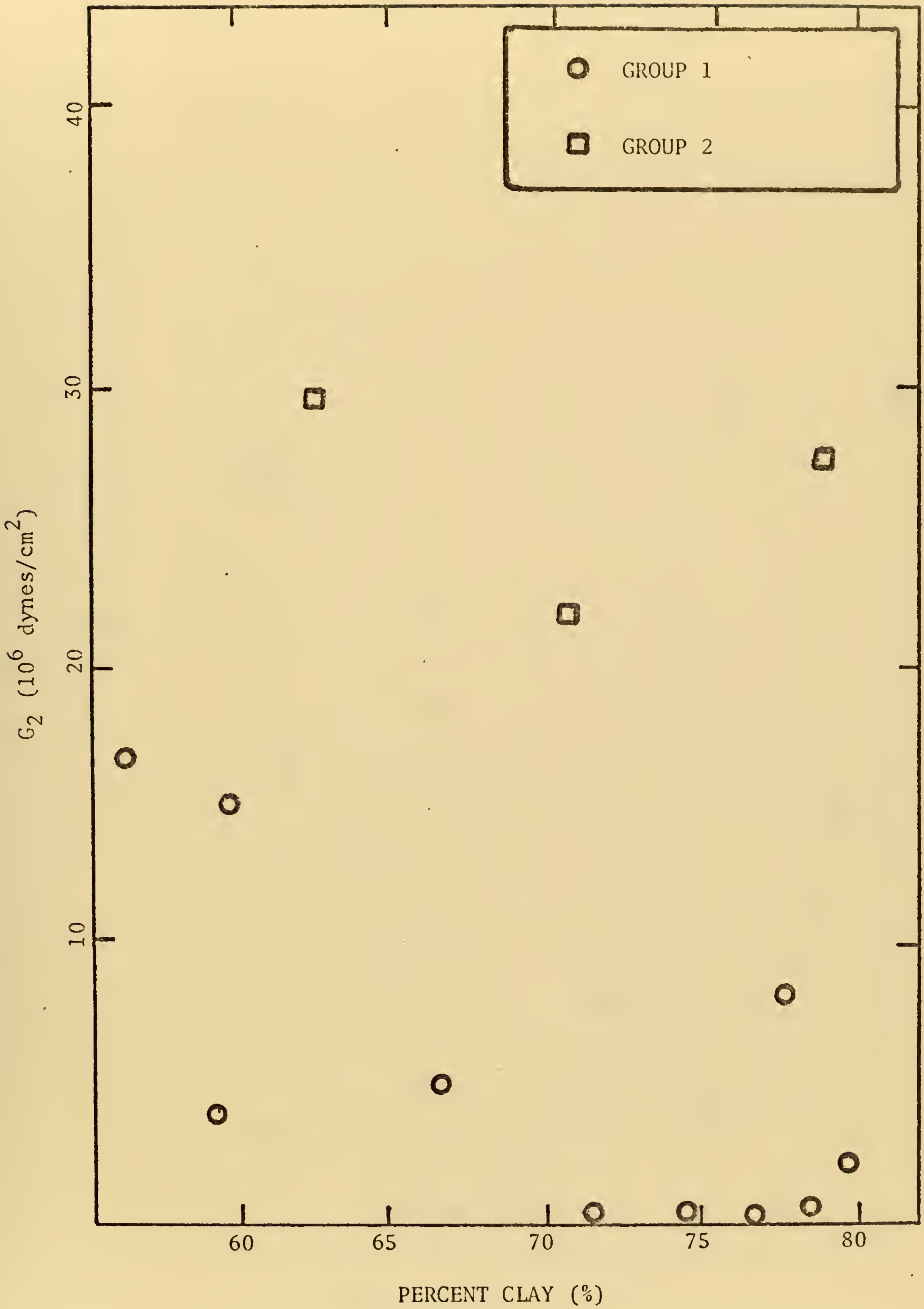

Figure 30. G_2 as a Function of Percent Clay.

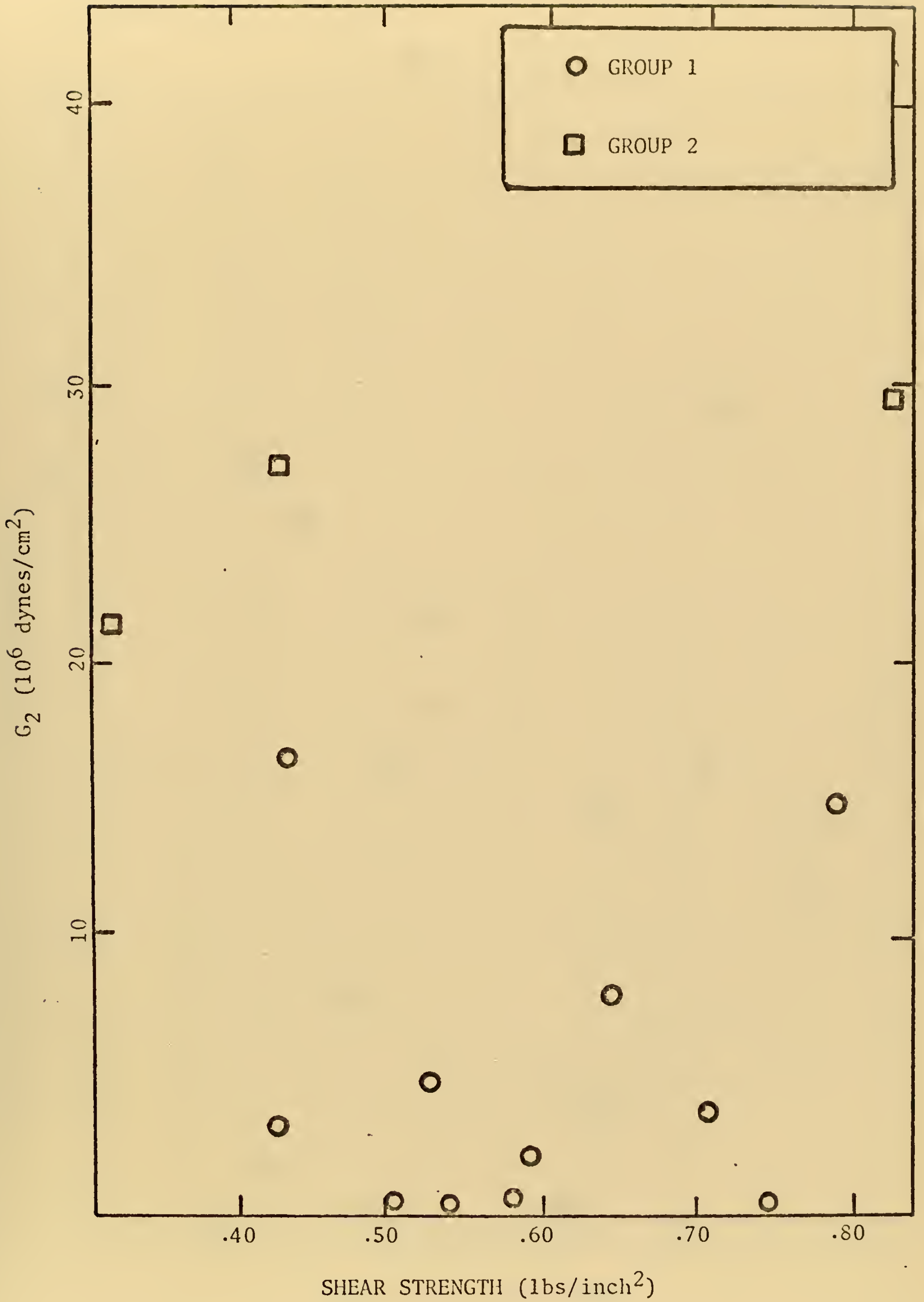

Figure 31. G_2 as a Function of Vane Shear Strength.

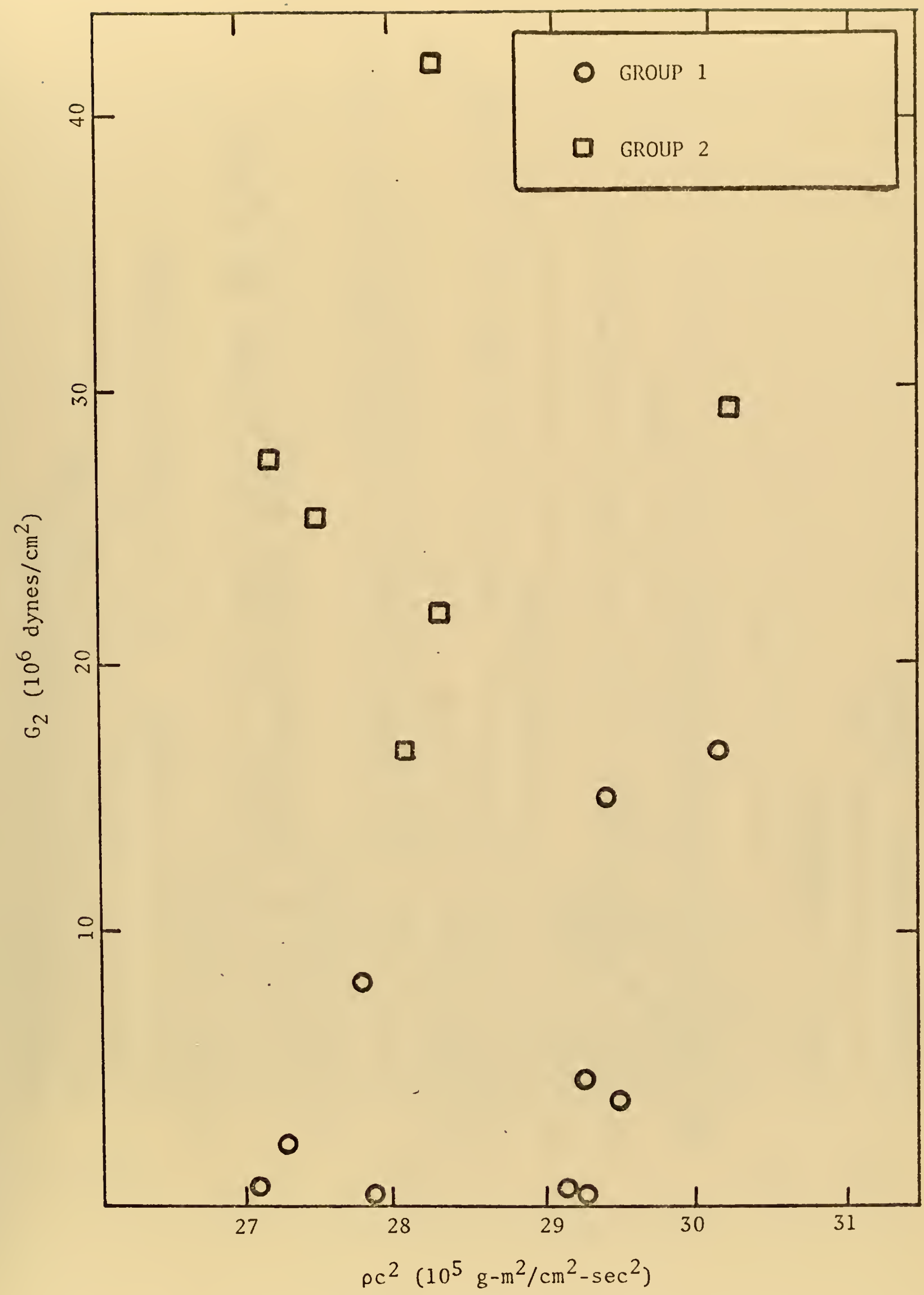

Figure 32. G_2 as a Function of the Product of Density and Sound Speed Squared.

```
C     PROGRAM KCAL
C     PROGRAM FOR CALCULATING K-ONE AND K-TWO
C      THIS PROGRAM WAS UTILIZED USING THE VISCOELASTOMETER IN A VACUUM
C     AND VARIOUS VISCOSITY OILS FOR CALIBRATION.
C     DATA CARD INPUT SHOULD BE AS FOLLOWS-  FVAC(F10.2),FSED(F10.2),
C      GVAC(F10.9), GSED(F10.9), ETAONE, ROSED, M, XLENTH,
C
      DIMENSION FVAC(8), FSED(8), GVAC(8), GSED(8), DELRE(8),
     1DELFR(8), DREL(8), DFRL(3), S(8), X(8),XKONE(8), XKTWO(8)
      READ (5,100) FVAC
  100 FORMAT (8F10.2)
      READ (5,100) FSED
C     FVAC,FSED, GVAC, AND GSED ARE READ AS ENTIRE ARRAYS AND AS SUCH,
C     DATA CARDS ARE REQUIRED. EXTRA DATA, ALTHOUGH READ, WILL NOT BE
C     PROCESSED. 'M' IS THE NUMBER OF DATA POINTS
      READ (5,101) GVAC
  101 FORMAT (8F10.2)
      READ (5,101) GSED
C
C     ETAONE IS THE REAL NEWTONIAN VISCOSITY IN POISE, ROSED IS THE DENSITY
C     OF THE FLUID, XLENTH IS THE LENGTH OF THE ROD.(METRIC UNITS)
C
      READ (5,102) ETAONE, ROSED, M, XLENTH
  102 FORMAT (2F10.6,I2,F10.5)
      WRITE (6,113)
  113 FORMAT (1H1,' BROOKFIELD OIL - 1030 CP - 1 1/2 INCH, 1/2 INCH TRAN
     1SDUCER')
      WRITE (6,103) ETAONE,ROSED,XLENTH
  103 FORMAT (1H0,'ETA 1 =',F10.4,5X,'RHO SED =',F10.4,5X,'LENGTH OF
     1PROBE =',F6.3)
      WRITE (6,104)
  104 FORMAT (1H0,4X,'FVAC',6X,'FSED',2X,'GVAC IN MICROMHOS',2X,
     1'GSED IN MICROMHOS')
      DO 106 I=1,M
      WRITE (6,105) FVAC(I), FSED(I), GVAC(I), GSED(I)
  105 FORMAT (2F10.2,6X,F10.2,9X,F10.2)
  106 CONTINUE
      DO  107 I=1,M
C
C     FORM RE = 1/G AND PUT IN G ARRAYS
C
      GVAC(I) = 1/GVAC(I)
      GSED (I) = 1/GSED(I)
C
C     FORM THE DIFFERENCES, DELRE
C
      DELRE(I) = GSED(I) - GVAC(I)
      DELFR(I) = FVAC(I) - FSED(I)
```

```
C
C     CALCULATE THE REMAINING QUANTITIES
C
      DREL(I) = DELRE(I)/XLENTH
      DFRL(I) = DELFR(I)/XLENTH
      S(I) = (ROSED*3.1416*FSED(I)*ETAONE)
      X(I) = SQRT (S(I))
      XKONE(I) = DREL(I)/X(I)
  107 XKTWO(I) = DFRL(I)/X(I)
      WRITE (6,108)
  108 FORMAT (1H1,4X,'FSED',6X,'RE VAC',4X,'RE SED',2X,'DELTA RE',
     1'  -DELTA F',2X,'DEL RE/L',2X,'DEL FR/L',5X,'R = X',2X,'K 1(X10 E6
     2)',3X,'K 2(X10 E6)')
      DO 110 I = 1,M
      WRITE (6,109) FSED(I), GVAC(I), GSED(I), DELRE(I),DELFR(I),
     1DREL(I), DFRL(I),X(I),XKONE(I),XKTWO(I)
  109 FORMAT (1H0,F10.2,3F10.3,F10.2,2F10.5,F10.2,2X,6PF10.5,4X,
     16PF10.5)
  110 CONTINUE
C
C     NOW, CALCULATE THE AVERAGE K VALUES
C
      A = 0
      B = 0
      DO 111 I = 1,M
      A = A + XKONE(I)
      B = B + XKTWO(I)
      C = A/M
      D = B/M
  111 CONTINUE
      WRITE (6,112) C,D
  112 FORMAT (1H0,'AVERAGE K 1 (X10 E6) =',6PF10.5,'AVERAGE K 2 (X10 E6)
     1 =',6PF10.5)
      STOP
      END
```

```
C     PROGRAM RESCALC
C     PROGRAM FOR RESONANCE METHOD CALCULATION
C
      REAL*8 TITLE
      DIMENSION FVAC(8),FSED(8),GVAC(8),GSED(8),DELRE(8),DELFR(8),
     1DFRL(8),XKONE(8),XKTWO(8),R(8),X(8),GONE(8),GTWO(8),ETAONE(8),
     2ETATWO(8),DREL(8)
      READ (5,100)N,M
C
C     THIS PROGRAM CALCULATES, WITH ONE SET OF VACUUM READINGS, G'S AND ETA'S
C     FOR SEVERAL SETS OF SEDIMENT DATA. A RUN IS THE CALCULATION OF G'S AND
C     ETA'S FOR ONE SET OF DATA. 'M' IS THE NUMBER OF DATA POINTS PER RUN. 'M'
C     MUST BE THE SAME FOR EACH RUN.
C
  100 FORMAT (2I2)
      READ (5,101) FVAC
C
C     FVAC, FSED, GVAC, K1 ANDK2 ARE READ IN AS ENTIRE ARRAYS AND ENTIRE ARRAYS
C     MUST BE SUPPLIED. IF THE NUMBER OF DATA POINTS IS 6, READ IN  8 BITS OF
C     DATA. THUS THE LAST TWO NUMBERS OF EACH ARRAY WILL NOT BE UTILIZED.
C
  101 FORMAT(8F10.2)
      READ (5,102) GVAC
  102 FORMAT (8F10.2)
      READ (5,103) XKONE
  103 FORMAT (8F10.9)
      READ (5,103) XKTWO
 1031 READ (5,1032) XLENTH
 1032 FORMAT (F10.5)
      WRITE (6,104)
  104 FORMAT (1H1,'1 1/2 INCH, 1/2 INCH DIAMETER TRANSDUCER')
      WRITE (6,105)
  105 FORMAT (1H0,' M    FVAC',8X,'GVAC IN MICROMHOS',5X,'K 1',9X,'K 2')
      DO 107 I=1,M
      WRITE (6,106) I,FVAC(I),GVAC(I),XKONE(I),XKTWO(I)
  106 FORMAT (1H0,I2,F9.1,7X,F10.2,11X,F11.9,2X,F11.9)
C     FORM REVAC = 1/GVAC AND PUT INTO GVAC ARRAY
      GVAC(I) = 1.0/GVAC(I)
  107 CONTINUE
      DO 119 J=1,N
C
C     DATA READ FROM THIS POINT IS FOR A SINGLE RUN. THE NUMBERS OF SETS OF
C     THESE DATA MUST MATCH 'N'.
C
      READ (5,101) FSED
      READ (5,103) GSED
      READ (5,110) ROSED,TITLE
  110 FORMAT (F10.5,A8)
```

```
C
C     ROSED IS THE SEDIMENT DENSITY IN GMS/CC, XLENTH IS THE LENGTH OF THE ROD
C     IN CENTIMETERS.
C
      WRITE (6,111) J,TITLE
  111 FORMAT (1H1,' RUN NUMBER ',I2,3X,'CORE ',A8)
      WRITE (6,112) ROSED, XLENTH
  112 FORMAT (1H0,' ROSED = ',F7.4,5X,'ROD LENGTH = ',F6.3)
      WRITE (6,113)
  113 FORMAT (1H0,' M   F SED',5X,'G SED IN MICROMHOS')
      DO 115 I=1,M
      WRITE (6,114) I,FSED(I),GSED(I)
  114 FORMAT (1H0,I2,F10.2,6X,F10.2)
C     FORM RESED = 1/GSED AND PLACE IN GSED ARRAY
      GSED(I) = 1.0/GSED(I)
C     FORM DIFFERENCES
      DELRE(I) = GSED(I) - GVAC(I)
      DELFR(I) = FVAC(I) - FSED(I)
C     CALCULATING THE REMAINING QUANTITIES
      DREL(I) = DELRE(I)/XLENTH
      DFRL(I) = DELFR(I)/XLENTH
      R(I) = DREL(I)/XKONE(I)
      X(I) = DFRL(I)/XKTWO(I)
      GONE(I) = (R(I)**2 - X(I)**2)/ROSED
      GTWO(I) = 2.0*R(I)*X(I)/ROSED
      ETAONE(I) = GTWO(I)/(6.2832*FSED(I))
      ETATWO(I) = GONE(I)/(6.2832*FSED(I))
  115 CONTINUE
      WRITE (6.116)
  116 FORMAT(1H1,' M',2X,'FSED',5X,'RE VAC',4X,'RE SED',2X,'DELTA RE',
     1'  -DELTA F','  DEL RE/L  -DEL FR/L',6X,'R',7X,'X',6X,'ETA 1',5X,
     2'ETA 2',8X,'G 1',8X,'G 2')
      DO 118 I=1,M
      WRITE (6.117) I,FSED(I),GVAC(I),GSED(I),DELRE(I),DELFR(I),DREL(I),
     1DFRL(I).R(I).X (I),ETAONE(I),ETATWO(I),GONE(I),GTWO(I)
  117 FORMAT (1H0,I2,F9.2,F9.6,2F10.7,F9.2,F10.7,F10.5,F10.3,F9.3,F9.4,
     1F10.4,2F11.1)
  118 CONTINUE
  119 CONTINUE
       STOP
      END
```

BIBLIOGRAPHY

1. Anderson, R. S. and G. V. Latham, Determination of Sediment Properties from First Shear Mode Rayleigh Waves Recorded on the Ocean Bottom, *Journal of Geophysical Research*, v. 74, no. 10, 1969, 2747-2757.

2. Bieda, G. E., Measurement of the Viscoelastic and Related Mass-Physical Properties of Some Continental Terrace Sediments, *M.S. Thesis, Naval Postgraduate School*, 1970.

3. Bucker, H. P., J. A. Whitney, G. S. Yee and R. R. Gardner, Reflection of Low-Frequency Sonar Signals from a Smooth Ocean Bottom, *The Journal of the Acoustical Society of America*, v. 37, no. 6, 1965, 1037-1051.

4. Cepek, R. J., Acoustical and Mass Physical Properties of Deep Ocean Recent Marine Sediments, *M.S. Thesis, Naval Postgraduate School*, 1972.

5. Cohen, S. R., Measurement of the Viscoelastic Properties of Water Saturated Clay Sediments, *M.S. Thesis, Naval Postgraduate School*, 1968.

6. Davies, D., Dispersed Stoneley Waves on the Ocean Bottom, *The Bulletin of the Seismological Society of America*, v. 55, no. 5, 1965, 903-918.

7. Gallagher, J. J. and V. A. Nacci, Investigations of Sediment Properties in Sonar Bottom Reflectivity Studies, *Underwater Sound Laboratory Report No. 944*, 1968.

8. Hamilton, E. L., Sound Velocity, Elasticity and Related Properties of Marine Sediments, North Pacific, Part I; Sediment Properties, Environmental Control, and Empirical Relationships, *Naval Undersea Research and Development Center Technical Report No. 143*, 1969.

9. Hamilton, E. L., Sound Velocity, Elasticity and Related Properties of Marine Sediments, North Pacific, Part II; Elasticity and Elastic Constants, *Naval Undersea Research and Development Center Technical Report No. 144*, 1969.

10. Hamilton, E. L., H. P. Bucker, D. L. Keir and J. A. Whitney, In Situ Determinations of the Velocities of Compressional and Shear Waves in Marine Sediments from a Research Submersible, *Naval Undersea Research and Development Center Technical Report No. 163*, 1969.

11. Hutchins, J. R., Investigation of the Viscoelastic Properties of a Water Saturated Sediment, *M.S. Thesis, Naval Postgraduate School*, 1967.

12. Lambe, T. W., Soil Testing for Engineers, p. 165, John Wiley & Sons, 1951.

13. Mason, W. P., Measurements of the Viscosity and Shear Elasticity of Liquids by Means of a Torsionally Vibrating Crystal, Transactions of the A. S. M. E., May 1947, 359-370.

14. Mason, W. P., Physical Acoustics, v. 2, part B, Academic Press, 1965.

15. McSkimin, H. J. Measurements of Dynamic Shear Viscosity and Stiffness of Viscous Liquids by Means of Traveling Torsional Waves, The Journal of the Acoustical Society of America, v. 24, no. 4, 1952, 355-365.

16. Richart, F. E., Jr., J. R. Hall, Jr. and R. D. Woods, Vibrations of Soils and Foundations, Prentice-Hall, Inc., 1970.

17. Wilde, P., Recent Sediments of the Monterey Deep-Sea Fan, University of California Hydraulics Engineering Laboratory Technical Report No. HEL 2-13, 1965.

18. Wilson, O. B., Jr. and R. S. Andrews, Measurement of the Dynamic Rigidity of Sediments, Proceedings International Symposium on the Engineering Properties of Sea-Floor Soils and Their Geophysical Identification, Seattle, Washington, pp. 75-94A, 1971.

INITIAL DISTRIBUTION LIST

		No. Copies
1.	Defense Documentation Center Cameron Station Alexandria, Virginia 22314	2
2.	Library, Code 0212 Naval Postgraduate School Monterey, California 93940	2
3.	Professor O. B. Wilson, Jr., Code 61Wl Department of Physics Naval Postgraduate School Monterey, California 93940	5
4.	Professor R. S. Andrews, Code 58Ad Department of Oceanography Naval Postgraduate School Monterey, California 93940	5
5.	Department of Oceanography, Code 58 Naval Postgraduate School Monterey, California 93940	3
6.	Office of Naval Research Code 480D Arlington, Virginia 22217	1
7.	Oceanographer of the Navy The Madison Building 732 N. Washington Alexandria, Virginia 22314	1
8.	Dr. William R. Bryant Texas A&M University Department of Oceanography College Station, Texas 77843	1
9.	Dr. Davis A. Fahlquist Texas A&M University Department of Geophysics College Station, Texas 77843	1
10.	Dr. E. L. Hamilton Naval Undersea Research and Development Center San Diego, California 92152	1
11.	LCDR R. J. Cepek, USN NAVSECREP Massawa MAAG Ethiopia APO New York 09843	1

		No. Copies
12.	LTjg G. A. Engel c/o Ernest J. Engel Box 25 North Platte, Nebraska 69101	2
13.	Homa Lee Naval Civil Engineering Laboratory Port Hueneme, California 93043	1

DOCUMENT CONTROL DATA - R & D

(Security classification of title, body of abstract and indexing annotation must be entered when the overall report is classified)

ORIGINATING ACTIVITY *(Corporate author)* Naval Postgraduate School Monterey, California 93940	2a. REPORT SECURITY CLASSIFICATION Unclassified 2b. GROUP

REPORT TITLE

Measurement of the Complex Dynamic Rigidity of Recent Marine Sediments

DESCRIPTIVE NOTES *(Type of report and inclusive dates)*

Master's Thesis; December 1972

AUTHOR(S) *(First name, middle initial, last name)*

Gregory A. Engel

REPORT DATE December 1972	7a. TOTAL NO. OF PAGES 82	7b. NO. OF REFS 18

a. CONTRACT OR GRANT NO.	9a. ORIGINATOR'S REPORT NUMBER(S)
b. PROJECT NO.	
c.	9b. OTHER REPORT NO(S) *(Any other numbers that may be assigned this report)*
d.	

10. DISTRIBUTION STATEMENT

Approved for public release; distribution unlimited.

11. SUPPLEMENTARY NOTES	12. SPONSORING MILITARY ACTIVITY Naval Postgraduate School Monterey, California 93940

13. ABSTRACT

The dynamic rigidity of 17 samples of continental terrace clayey-silt sediments has been measured in the laboratory using a viscoelastometer in the frequency range of 7 to 60 kHz. The method involves the propagation of torsional waves on a rod and measuring the effects of shear loading imparted to the rod when imbedded in a sediment. Values of the real component of rigidity range from 1.6 X 10^6 dynes/cm^2 to 2.1 X 10^7 dynes/cm^2. Values of the imaginary component of rigidity range from 2.0 X 10^5 dynes/cm^2 to 4.1 X 10^7 dynes/cm^2. No clear-cut dependence of rigidity upon frequency is observed. Both real and imaginary components of rigidity are analyzed by plotting the data as a function of various other mass-physical properties, including: density, porosity, compressional wave speed, sand-silt-clay percentages, vane shear strength, and the product of density and sound speed squared. These analyses substantiate research done by other workers indicating that both real and imaginary components of rigidity exhibit trends with some of the mass-physical properties.

14 KEY WORDS	LINK A		LINK B		LINK C	
	ROLE	WT	ROLE	WT	ROLE	WT
viscoelastic						
shear modulus						
dynamic rigidity						
sediment						

DD FORM 1 NOV 65 1473 (BACK)
S/N 0101-807-6821

Thesis 141285
E445 Engel
c.1 Measurement of the complex dynamic rigidity of recent marine sediments.